AFRL-AFOSR-VA-TR-2022-0051

Inlet Isolator and Combustor Physics at Take-Over Region of Scramjet Engines

Lee, Tonghun
UNIVERSITY OF ILLINOIS
352 HENRY ADMINISTRATION BLDG
URBANA, IL, 61801
USA

09/16/2021
Final Technical Report

Air Force Research Laboratory
Air Force Office of Scientific Research
Arlington, Virginia 22203
Air Force Materiel Command

REPORT DOCUMENTATION PAGE

Form Approved
OMB No. 0704-0188

1. REPORT DATE *(DD-MM-YYYY)*	**2. REPORT TYPE**	**3. DATES COVERED** *(From - To)*
16-09-2021	Final	15 Dec 2016 - 14 Jun 2021

4. TITLE AND SUBTITLE
Inlet Isolator and Combustor Physics at Take-Over Region of Scramjet Engines

5a. CONTRACT NUMBER

5b. GRANT NUMBER
FA9550-17-1-0008

5c. PROGRAM ELEMENT NUMBER
61102F

6. AUTHOR(S)
Tonghun Lee

5d. PROJECT NUMBER

5e. TASK NUMBER

5f. WORK UNIT NUMBER

7. PERFORMING ORGANIZATION NAME(S) AND ADDRESS(ES)
UNIVERSITY OF ILLINOIS
352 HENRY ADMINISTRATION BLDG
URBANA, IL 61801
USA

8. PERFORMING ORGANIZATION REPORT NUMBER

9. SPONSORING/MONITORING AGENCY NAME(S) AND ADDRESS(ES)
AF Office of Scientific Research
875 N. Randolph St. Room 3112
Arlington, VA 22203

10. SPONSOR/MONITOR'S ACRONYM(S)
AFRL/AFOSR RTA1

11. SPONSOR/MONITOR'S REPORT NUMBER(S)
AFRL-AFOSR-VA-TR-2022-0051

12. DISTRIBUTION/AVAILABILITY STATEMENT
A Distribution Unlimited: PB Public Release

13. SUPPLEMENTARY NOTES

14. ABSTRACT
This report outlines an effort to understand the impact of inlet isolator physics on the combustion of scramjet engines under actual flight relevant conditions in the take-over regime. We strive to answer the fundamental question “what basic physics underlying the connection between inlet isolator physics and combustion stability in canonical axisymmetric and/or rectangular geometries are applicable to more practical systems?” More specifically, the objective of the proposed work is to gain a fundamental understanding of the feedback mechanism between the boundary layer structures and separated flow in the isolator and the corresponding combustion dynamics that can lead to instabilities and/or unstart. An experimental effort is proposed where unstart and combustion instabilities are investigated in an optically accessible axisymmetric scramjet model in a free flow high enthalpy flow tunnel. The effort will be coupled with advanced spatially resolved diagnostics of both the isolator and the combustor region to obtain critical insight into the key physics, and potentially evolve into a foundational platform numerical analysis in the future.
A

15. SUBJECT TERMS

16. SECURITY CLASSIFICATION OF:			**17. LIMITATION OF ABSTRACT**	**18. NUMBER OF PAGES**	**19a. NAME OF RESPONSIBLE PERSON**
a. REPORT	**b. ABSTRACT**	**c. THIS PAGE**			CHIPING LI
U	U	U	UU	33	**19b. TELEPHONE NUMBER** *(Include area code)* 426-8574

FINAL REPORT

INLET ISOLATOR AND COMBUSTOR PHYSICS AT TAKE-OVER REGION OF SCRAMJET ENGINES

AFOSR Grant Number: FA9550-17-1-0008

September 2021

Tonghun Lee
Professor
Department of Mechanical Science & Engineering
University of Illinois at Urbana-Champaign
1206 W. Green Street,
Urbana, IL 61801-2906

Venkat Narayanaswamy (Co-PI, subcontract)
Assistant Professor
Department of Mechanical and Aerospace Engineering
North Carolina State University
911 Oval Drive, EM3, Rm. 3292
Raleigh, NC 27695

1. ABSTRACT

This report outlines an effort to understand the impact of inlet isolator physics on the combustion of scramjet engines under actual flight relevant conditions in the take-over regime. We strive to answer the fundamental question "***what basic physics underlying the connection between inlet isolator physics and combustion stability in canonical axisymmetric and/or rectangular geometries are applicable to more practical systems?***" More specifically, the objective of the proposed work is to gain a fundamental understanding of the feedback mechanism between the boundary layer structures and separated flow in the isolator and the corresponding combustion dynamics that can lead to instabilities and/or unstart. An experimental effort is proposed where unstart and combustion instabilities are investigated in an optically accessible axisymmetric scramjet model in a free flow high enthalpy flow tunnel. The effort will be coupled with advanced spatially resolved diagnostics of both the isolator and the combustor region to obtain critical insight into the key physics, and potentially evolve into a foundational platform numerical analysis in the future.

A robust and detailed characterization of the complex phenomena involved with scramjet choking required a systematic year-by-year approach. Year 1 focused heavily on controlled experiments of combustion-induced choking, specifically characterizing pseudoshock development and propagation in a simple axisymmetric flowpath in a direct connect configuration of the newly developed high enthalpy wind tunnel, ACT-2. In addition, work began on the design and preliminary testing of a more complex, fully-integrated inlet-isolator-combustor constant area axisymmetric scramjet model that could be tested in the semi-freejet configuration of the ACT-2. Year 2 saw a more comprehensive effort towards the characterization of the semi-freejet choking behavior at both high and low enthalpy conditions for reacting and non-reacting cases, including isolator shock train behavior and combustor pseudoshock stability during mode transition. Additionally, shock train dynamics in a rectangular geometry was explored at low enthalpy revealing the differences betwee axisymmetric and three-dimensional pseudoshock behaviors. Year 3 brought the lessons learned in the constant area axisymmetric scramjet geometry to bear, as different non-canonical design features such as a flameholding cavity and diverging combustor walls were implemented and tested. 1-D analysis provided insight into the design process and validation between the experimental results and theory. The combustion performance using enhanced design features was assessed, with an emphasis on choking thresholds and pseudoshock propagation. Finally, a novel three-dimensional flowpath geometry, the perisymmetric scramjet, was proposed and tested over the course of Year 3 into the final year of the project. Results of these experiments were parametrically compared to that of the canonical axisymmetric scramjet, which has served as the driving control geometry through the duration of the program.

2. INTRODUCTION

A canonical scramjet geometry, such as a constant area axisymmetric flowpath, allows for the study of fundamental aspects of supersonic combustion without the influence of complex flow interactions produced by dimensional changes of the flowpath. However, practical scramjet flowpaths should be designed to produce stable and efficient (i.e. minimal total pressure losses) combustion and sufficient heat release to net adequate thrust at flight conditions. Various modifications to features of a scramjet flowpath geometry can be implemented and optimized to

achieve this result, which would enhance its performance relative to a more canonical geometry. A pair of supersonic combustor design features that are integral to the success of scramjet performance are flameholding combustor wall cavities and diverging combustor walls. While the high-level effects of these features are well-understood, their impact on combustor performance when compared to the constant area, unmodified geometry has not been fully experimentally quantified.

Flame stability of hydrocarbon reactions have been a major challenge in the development of practical supersonic combustors [1]. The ignition, flame holding and combustion stabilization for hydrocarbon fuels are challenging in scramjet combustors because the characteristic reaction time scales of hydrocarbon fuels tend to be longer than the supersonic flow residence time. Hydrocarbon fuels are favorable candidates for scramjet propulsion due to their high energy density, general availability and easier handling [2]. Combustor wall cavities have long been used as integrated fuel injection/flame-holding approaches for supersonic flame stabilization and combustion performance improvement in scramjet engines due to their minimal system complexity and performance detriment (i.e., total pressure losses) [3]. Wall cavities in scramjet combustors can increase flow residence time and enhance fuel/air mixing rate by creating low-speed recirculation regions and pools of hot radicals that reduce the induction time of chemical reactions and serve as self-sustaining ignition sources [4]. The cavity flame-holding phenomena have been widely studied with various fueling schemes and mixing enhancement strategies in rectangular direct-connect supersonic combustors [5-7] and rectangular scramjet models [8].

Diverging walls serve to enhance the thrust-generating potential of a scramjet by increasing the amount of possible combustion and heat release in the combustor and staving off the onset of performance degrading boundary layer separation by relieving the combustion-induced pressure rise. According to one-dimensional flow with heat release (Rayleigh flow), a constant area combustor can only sustain a finite amount of heat release before the flow is driven to Mach 1 at the exit, resulting in choked flow. Area divergence extends the threshold for choking, allowing for more fuel to be burned in the combustor than in a purely constant area combustor. Billig developed a quasi-one-dimensional pressure-area relation that analytically determined the maximum area divergence of a supersonic combustor for maximum combustion efficiency (i.e. minimum entropy rise), which would result in sonic conditions at the exit of the combustor [9]. It can be said that for a large range of flight Mach numbers, area divergence is necessary to generate the maximum amount of heat release through combustion and net the greatest potential for thrust.

There has been an increase in the interest in axisymmetric and elliptical geometries in their use in practical scramjet flowpaths [10-16]. The benefits of such scramjet combustors compared with rectangular combustors include undesirable effects from the hypersonic corner boundary-layer effects, the increased structural efficiency, decreased structural weight required to withstand a specified pressure/thermal load and the reduced wetted surface area needed to enclose a specific cross-sectional area. Gruber et al. [4] characterized the flowpaths of a hydrocarbon-fueled axisymmetric scramjet combustor with a wide operation range in a direct-connect supersonic combustion facility. Smart and Trexler [10] proposed a hypersonic inlet with rectangular-to-elliptical shape transition (REST) and tested the inlet performance in combination with an elliptical combustor. Denman et al. [12] investigated the supersonic combustion of hydrocarbon fuels and cavity flame-holding ability inside the scramjet with REST inlet at Mach 8 flight conditions. Due to intrinsic limitations from complicated curved surface design/fabrication and test facility operation conditions, optical accesses into the elliptical or axisymmetric scramjet models have remained a significant challenge though it is necessary for investigation on internal flow and

combustion dynamics in combustors. A new archetype of flowpath geometry inspired by both the axisymmetric and elliptical geometries, the perisymmetric geometry, is proposed as a potentially viable scramjet geometry. It combines the manufacturability of the axisymmetric geometry and the improved injection penetration potential of the elliptical geometry. Additionally, it might be supposed that the presence of corner flow effects may enhance the fuel-air mixing processes in the combustor.

While the internal aerodynamics of hypersonic scramjet propulsion has been extensively studied, one topic that eludes adequate characterization is that of its principal failure mode: inlet unstart. Inlet unstart results in a catastrophic degradation of engine performance and total loss of net thrust. In 2011, the flight of the X-51A, an experimental scramjet-powered vehicle, failed due to unstart of its scramjet engine right after ignition [17]. In unstarted conditions, a normal shock stands in front of the inlet, usually accompanied by large flow spillage that reduces the engine air supply. The engine is incapable of providing useful thrust and massive wave drag is produced by the choked inlet. Both external and internal factors can cause an inlet to unstart. External factors are mainly related to the flight conditions of the vehicle and may include a reduction of the free stream Mach number, excessive flow distortion (angularity, non-uniformity, etc.), pressure losses induced by shock waves or boundary layer separation, etc. Internal factors are mainly related to backpressure rise inside the engine as consequence of boundary layer separation or flow choking or a combination of the two. Choking occurs when at a certain location in the flow field the Mach number is lowered below unity and therefore is more likely to happen when the scramjet is operating at low Mach number ranges, typically from 4 to 7.

Choking can be caused by a variety of phenomena like combustion heat release (thermal choking), area blockage, mass injection, and/or flow irreversibilities. Once the flow is choked, a re-adjustment of the inflow is necessary to recover steady operations. According to one-dimensional inviscid theory, this adjustment is accomplished by the upstream propagation of a single normal shock. In practice, due the viscous interaction with the wall boundary layer, the single shock is usually split in a train of bifurcated normal shocks and/or oblique shocks know as a *pseudo-shock* [18-21]. Pseudo-shocks have been classified in λ-type [21] (typical of lower Mach numbers) and *x*-type [22] (typical of higher Mach numbers) depending on their geometry. Unlike a single normal shock, a pseudo-shock can be stabilized in a constant area channel provided that its length is sufficient to accommodate the entire shock structure [23] (up 15 hydraulic diameters at high Mach numbers). A constant area channel between inlet and combustor can therefore be used to arrest the propagation of the pseudo-shock preventing it from reaching the inlet and causing unstart. Such devices are known as *constant area diffusers* or *isolators* [24].

A significant number of studies on unstart were conducted in low enthalpy supersonic facilities, inducing unstart artificially by area blockage [25-30] or mass injection [31-32]. These results cannot be directly extrapolated to realistic scramjet flows, however they greatly contributed to advance the knowledge on pseudo-shock structure and dynamics. The initiation mechanism of blockage-induced unstart is well understood. The blockage generates a large adverse pressure gradient that separates the boundary layer. The separated region interacts with the supersonic flow introducing shock compression (shock-train). As the blockage is increased, the separated region extends upstream and the overall compression on the supersonic flow becomes more and more severe until it chokes. A propagation of a pseudo shock initiates and under certain conditions the pseudo-shock can be arrested and confined in the isolator, but this is usually accompanied by severe longitudinal oscillations and pressure fluctuations [33-36].

Experiments of high enthalpy conditions with unstart initiated by combustion are less abundant due to the limited availability of facilities able to produce suitable flow conditions. It is well known that that constant area combustors at low inlet Mach numbers and high fuel concentrations are subjected to unstart. The phenomenon was initially explained as *thermal choking,* induced by an excessive combustion heat-release as predicted by Rayleigh theory. However, the *thermal choking* explanation proved to be not fully exhaustive. Frost *et al.* [37] observed unstart in a model of the HyShot scramjet at fueling rates at which the expected heat-release was insufficient to cause thermal choking, therefore they proposed boundary layer separation as triggering mechanism of unstart. Laurence *et al.* [38,39] performed similar tests on a model provided with optical access and showed that shock propagation began before separation was observed, ruling out separation as responsible mechanism for unstart initiation. They attributed unstart initiation to 'localized' thermal choking phenomena and suggested that steady, one-dimensional theories (like Rayleigh flow) are not adequate to describe the actual flow in a combustor due to its strong unsteadiness and three-dimensionality. Lee *et al.* proposed a description of the onset of choking which takes into account the higher dimensionality of choking flow, whereby he attributed the onset of global choking to a cascade of events triggered by boundary layer-localized shock formation along 'false-choke' lines. Other notable contributions to the study of unstart in reacting flows were given by O'Byrne *et al.* [40], Owens *et al.* [41] Mashio *et al.* [42] Do *et al.* [43] and Im *et al.* [31].

In the current work, an assessment of combustion performance with a diverging combustor with cavity is made, and in the scope of choking and unstart, choking threshold and pseudoshock propagation. Lastly, combustion studies in the newly proposed and developed perisymmetric scramjet geometry will be conducted to assess its performance against that of the canonical axisymmetric geometry.

3. EXPERIMENTAL SETUP IN ACT-II

A. The Arc-heated Combustion Tunnel ACT-II

The experiments are conducted in the ACT-II hypersonic facility (see Figure 1) of the University of Illinois at Urbana-Champaign. ACT-II is a pulsed, high-enthalpy (up to 4.5 MJ/kg), blowdown wind tunnel specifically designed for supersonic combustion research. The facility consists of two high-pressure tanks, where the working gases (nitrogen and oxygen) are initially stored, a hot-gas generator (arc-jet type), a converging-diverging (C/D) nozzle, a test-section/combustor and a vacuum tank where the gas is exhausted.

The arc-heater of ACT-II has a coaxial electrodes configuration with a cylindrical cathode (lanthanated tungsten) and an annular anode (TZM alloy), separated by a ceramic constrictor. A typical DC voltage of 550-600 V is initially applied between the electrodes, and when the gas is injected, an electric discharge is initiated by voltage breakdown. In normal operations the arc is ignited in argon and successively transitioned to nitrogen. Oxygen is injected downstream of the anode and mixed with the heated nitrogen using a set of ceramic screens. This injection method reduces the erosion of the electrodes (and the consequent contamination of the flow) by limiting the formation of atomic oxygen in the arc chamber. The mixture, equivalent to air composition, reaches thermodynamic equilibrium flowing at low speed through a plenum chamber and then is expanded to supersonic speed by the C/D nozzle. The nozzle can be directly connected to a combustor (direct-connect mode) or attached to a test-section to operate the facility in free-jet mode. Arc voltage and current, plenum pressure and mass flow rates of freestream and fuel are

acquired during each tunnel run. Depending on the flow conditions, the typical test time ranges between 500 and 1000 ms. Further details about the facility and its performance are provided in Refs. [44-46].

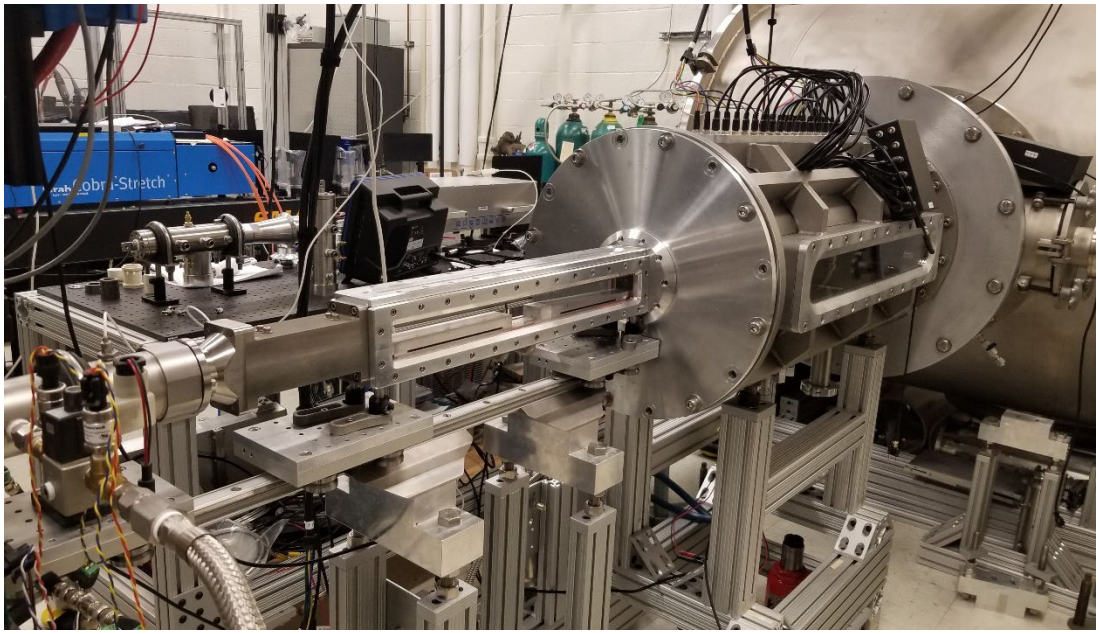

Figure 1. The ACT-II facility

B. Free-jet Configuration and Test Conditions

A free-jet type scramjet (Figure 2) is installed in the open-type test section of ACT-II facility. The axisymmetric (circular) scramjet model has an isolator of 254 mm in length, a combustor of 339 mm in length, and an internal flow channel of diameter 35 mm with a constant cross-section in the isolator and the combustor. The conical inlet has an aperture angle of 20 deg and provides flow compression by oblique shocks that continues throughout the isolator section.

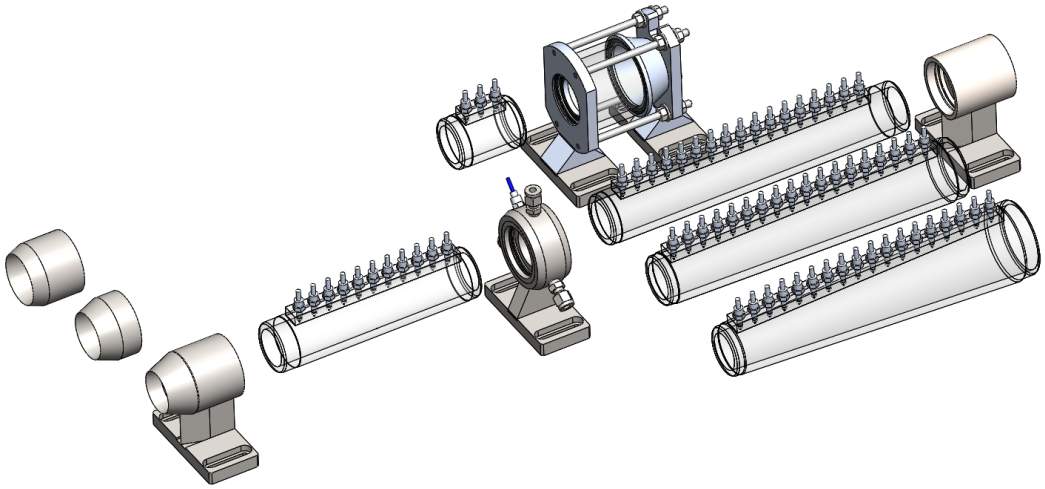

Figure 2. An overview of the scramjet model with three inlet options, as well as flameholding cavity and diverging combustor sections.

The inlet can be replaced to change the area contraction ratios (CR), available values of CR are 1.3, 1.6, and 1.9. An annular fuel injector is used to deliver the gaseous ethylene into the supersonic crossflow. The injector is composed by an annular collector provided with 16 sonic nozzles equally distributed in the circumferential direction. Each nozzle has a diameter of 0.75 mm and is vectored 45 deg downstream as in Figure 1a. A Kulite XTEL-190SM-50A sensor measures in real time the pressure inside the annular chamber during the test. This pressure is then used to compute the mass flow rate of gas injected using the sonic area relation. An axisymmetric cavity was designed to provide flameholding and enhanced mixing conditions at the start of the combustor. The cavity was designed with a length of 62 mm and a depth of 11 mm, with a closeout angle of 22.5°. Injection was maintained upstream of the cavity, providing an initial length for fuel-air mixing development before reaching the cavity.

Furthermore, diverging combustor geometries (matched length with the constant area combustor) were designed and tested. Total divergence angles of 2° and 5° were tested. These combustors were designed in a modular way that allowed interface with either the cavity or no-cavity configuration.

Combustors and isolator were instrumented with pressure transducers at the wall. The acrylic tubes are instrumented with 11 pressure transducers (Kulite XTE-190SM-5A) spaced 15 mm along the flow direction. The signal from the pressure transducers are filtered (20 kHz bandwidth) and amplified through Dataforth 8B50 signal conditioners and acquired by a National Instruments PCIe-6363 data acquisition system.

Quantitative measurements of the flow stagnation enthalpy and Mach number are taken at the combustor exit near the centerline. The Mach number is calculated from the simultaneous measurement of pitot and static pressure near the exit using the Rayleigh-Pitot formula. The pitot probe used consists of a metal tube (internal diameter 1.5 mm, outer diameter 4 mm, length 90 mm) with conical tip (30 deg) instrumented with a Kulite XTL-190-SM-5A pressure transducer. The stagnation enthalpy of the flow is evaluated from heat flux measurements at the stagnation point of a spherical probe using the Sutton and Graves correlation [47]. The heat flux probe is composed by a metal cylinder with spherical nose (Cu-Ni alloy, radius 2 mm) instrumented by a fast-response (1 μs) coaxial thermocouple Medtherm TCS-031-K flush mounted at the stagnation point. Further details about the calculation of Mach number and heat flux can be found in Ref. [48]. It is noteworthy that the pitot and heat flux probe are positioned in such a way to have negligible blockage effect on the combustor flow. Table 1 outlines the freestream conditions employed for the high-enthalpy tests.

Table 1. High Enthalpy Test Conditions

Freestream			
Stagnation Temperature	T_{t0}	2540	K
Stagnation Pressure	P_{t0}	118	kPa
Mach Number	M_1	4.48	-
Static Temperature	T_1	503	K
Static Pressure	P_1	407	Pa
Density	ρ_1	0.028	kg/m^3
Velocity	V_1	2023	m/s

C. Optical Setup for Flow Visualization

Three types of flow visualization are used in this study, hydroxyl (OH) planar laser induced fluorescence (PLIF) and high-speed plasma luminescence, and cold flow CO_2 planar laser Rayleigh scattering (PLRS).

Hydroxyl radicals, formed during high-temperature combustion, can be regarded as markers of combustion zones in supersonic reacting flows [49]. In this study, OH PLIF imaging is carried out to visualize the flame structure in the combustor of the model scramjet. The OH-PLIF setup is shown in Figure 3. The $Q_1(6)$ transition of the $A^2\Sigma^+$-$X^2\Pi$ (1,0) vibronic band of the OH molecule near 283 nm has been selected due to its low temperature-dependency [50]. A tunable dye laser Sirah Cobra-Stretch CBST-P doubled in frequency, and pumped with the second harmonic of a 10 Hz Nd:YAG laser Spectra-Physics Quanta-Ray Pro-250, has been used to produce the desired laser radiation with pulse energy of 25 mJ.

The laser beam is converted into a thin (< 0.5 mm) sheet via an optical system consisting of one cylindrical plano-concave lens (f = -30 mm) and two cylindrical plano-convex lenses (f = 125 mm and f = 500 mm respectively). The laser sheet is projected into the scramjet combustor section from the model exhaust, in opposite direction with respect to the flow. An intensified scientific complementary metal-oxide semiconductor (sCMOS) imaging camera (Andor iStar-sCMOS-18F-E3) is used to capture the laser-induced OH fluorescence with a gate width of 100 ns. The camera lens used for the imaging is an ultraviolet lens (Cerco UV 100 f/2.8) fitted with a narrow bandpass filter (Asahi Spectra, ZBPA310) centered at 310+/-5 nm that covers the wavelength of the laser-induced OH fluorescence.

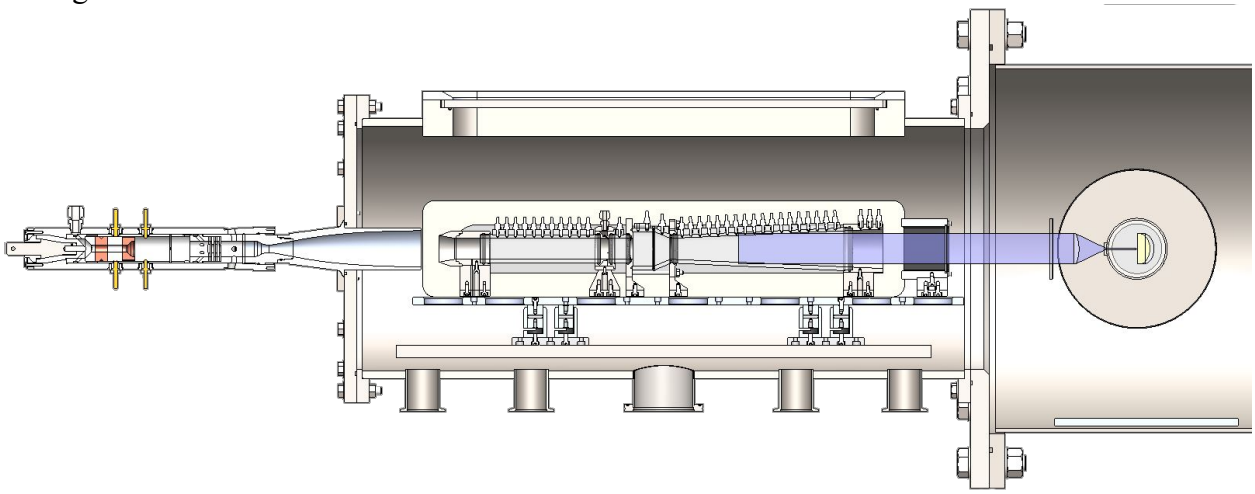

Figure 3. OH-PLIF optical setup in freejet-model configuration.

The natural luminescence of the hot plasma in the isolator is imaged using a high-speed camera (Photron Fastcam SA-5) provided with a 20 mm focal length lens. When the arc-heater is on, a fraction of the free electrons produced by the electric discharge is not able to recombine in the plenum chamber and survives the expansion through the nozzle. The free electrons contained in the freestream emit broadband radiation, mainly by *bremsstrahlung* interaction with the heavy particles. This emission can be exploited to visualize the flow. Despite line-of-sight integration, the images obtained revealed to be very effective in visualizing the structure of shocks. This technique is used in both reacting (fuel injection) and non-reacting cases (air injection) to study the dynamics of the flow in the isolator and the propagation of the pseudo-shock in the combustor.

4. RESULTS AND DISCUSSION

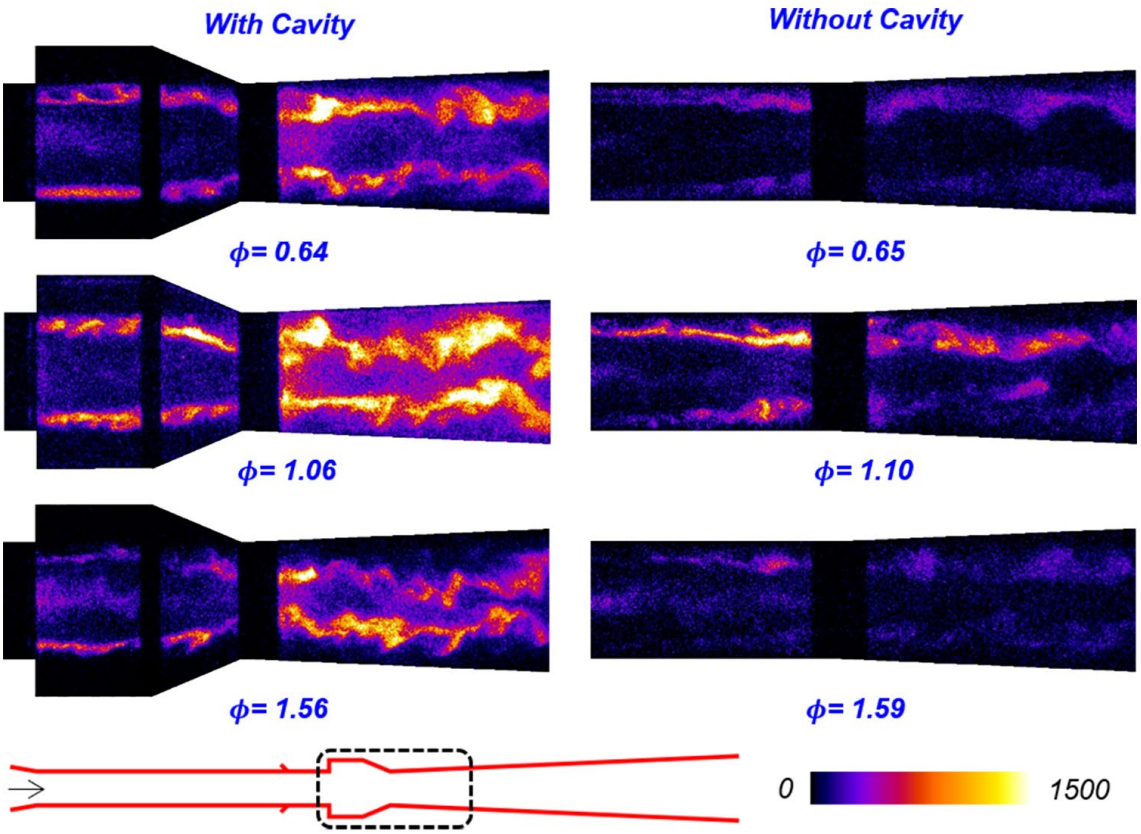

Figure 4. Effect of cavity on flame profile for a 5° diverging combustor in a generic axisymmetric scramjet design as observed using OH-PLIF

This section gives an overview of the experimental results obtained. The first compares the choking behavior induced by mass injection or heat release at high enthalpy conditions. Emphasizing lessons learned in the previous two sections, the next section focuses on a scramjet combustor design that optimizes combustion stability and efficiency.

A. Comparison of Choking Induced by Mass Injection and Heat Release at High Enthalpy

In this section, a comparison is made between the cases in which choking is induced by mass injection and by combustion, with the intent of understanding if the nature of blockage has any major effect on the flow dynamics. In order to make the comparison meaningful, air and fuel mass flow rates have been selected in such a way to produce the same average pressure profile in the isolator, as shown in Figure 5. It is useful to start the discussion having a look at the space-time pressure distribution inside the model scramjet. Figure 6 shows the pressure distribution for both non-reacting and reacting conditions. The plot covers the entire time lapse from the beginning of injection to the unstart of the inlet. The pressure data are plotted on space-time maps combining isolator and combustor.

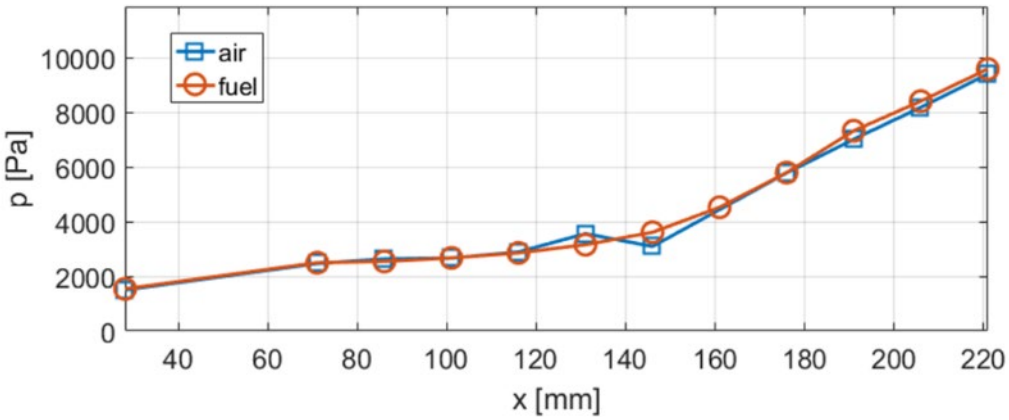

Figure 5. Average pressure distribution in the isolator with choked combustor. Comparison between choking induced by mass injection (blue) and by combustion (red).

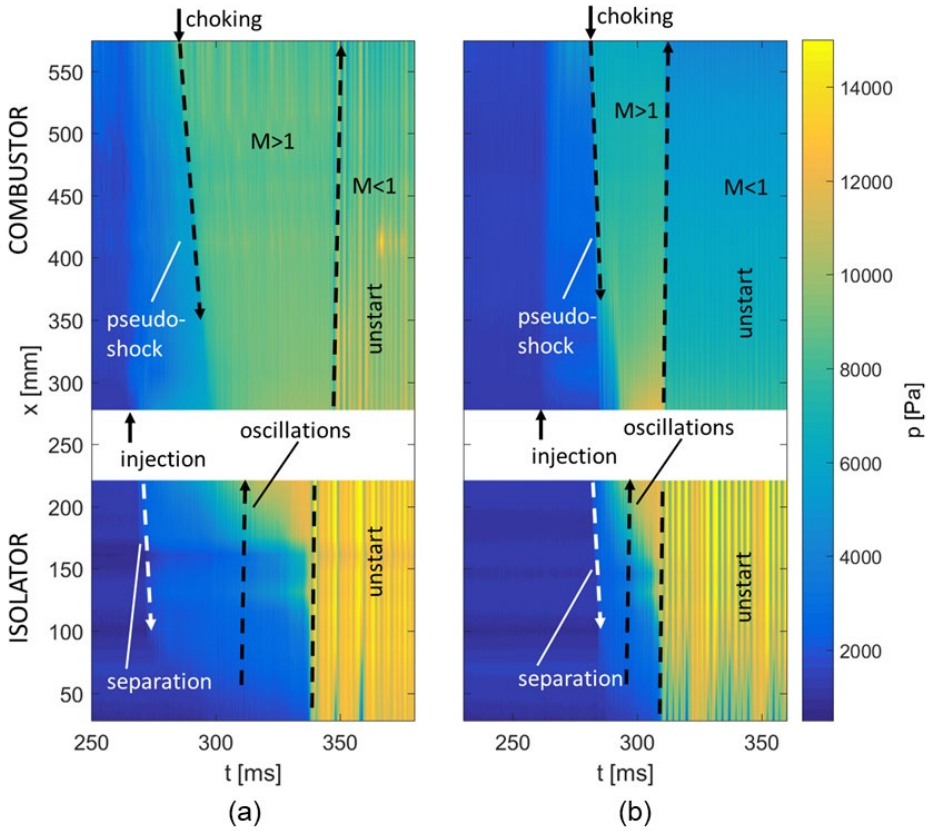

Figure 6. Isolator and combustor pressure contour in x-t space for conditions with unstart in a non-reacting (a) and reacting (b) flow.

The mass-choked (Figure 6a) and the combustion-choked (Figure 6b) pressure maps are very similar to each other and qualitatively similar to the low enthalpy mass-induced unstart case discussed in Ref. [51]. As injection is started, the blockage created by the jets induces boundary layer separation in the isolator and a shock-train is formed. Simultaneously, the pressure in the combustor rises until the flow chokes at the exit and a pseudo-shock is formed and starts

propagating upstream. When the pseudo-shock enters the isolator it starts interacting with the shock train, forcing self-sustained oscillations of the shock and pressure fluctuations. Ultimately the shock system reaches the inlet and disgorges outside. After unstart of the inlet, the flow becomes entirely subsonic throughout the model. Unlike the low-enthalpy case [51], the high-enthalpy subsonic flow is characterized by periodic pressure fluctuations.

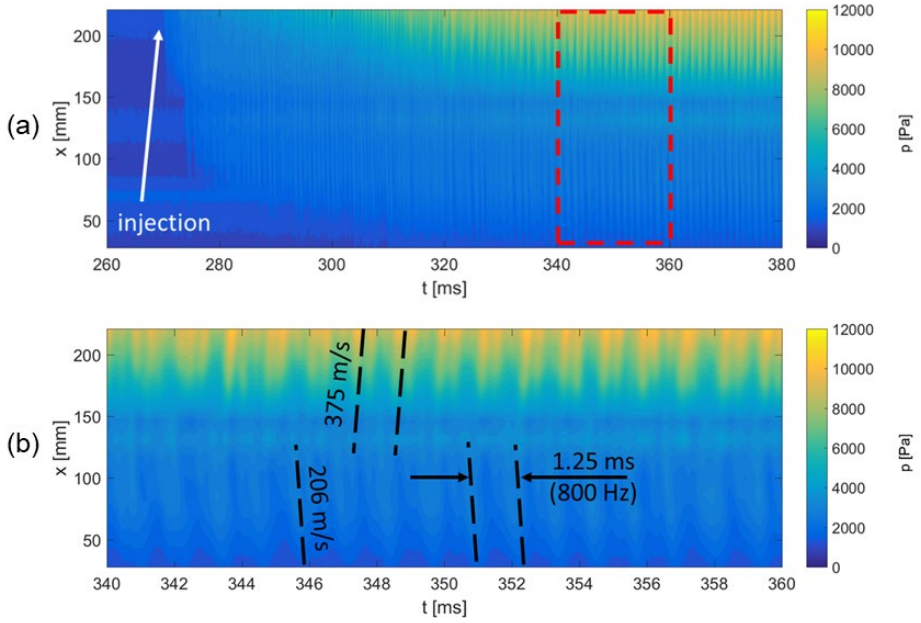

Figure 7. Pressure contour of the isolator pressure fluctuations in a x - t space for a non-reacting case. (a) Overview of the entire test. (b) Detailed view of 20 ms.

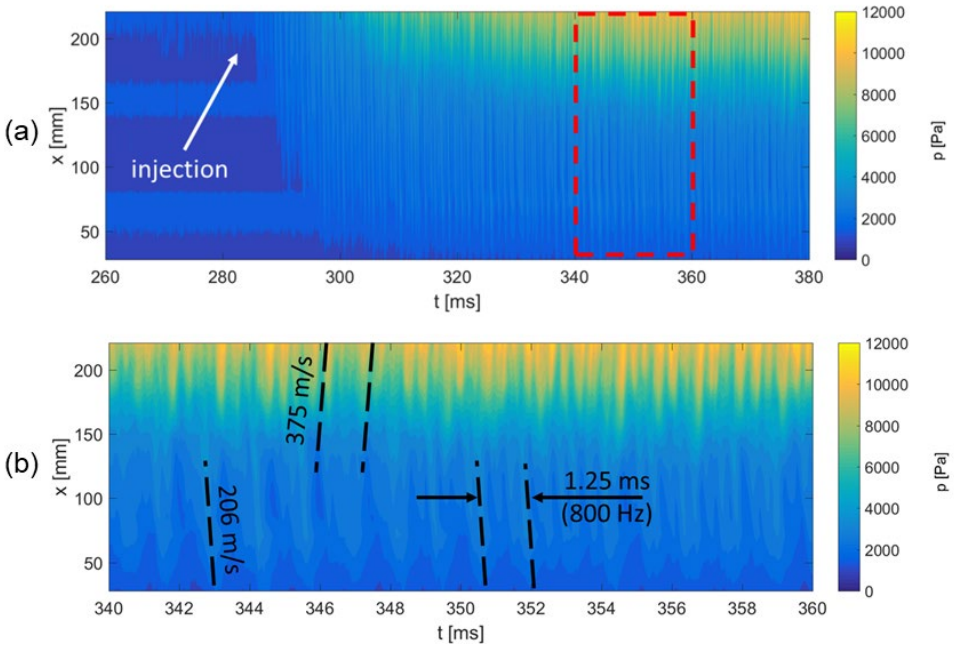

Figure 8. Pressure contour of the isolator pressure fluctuations in a x - t space for a reacting case. (a) Overview of the entire test. (b) Detailed view of 20 ms.

Reducing the level of blockage, unstart is avoided and the self-sustained shock oscillations continue indefinitely. An example is shown in Figure 8 for the reacting and in Figure 7 for the non-reacting flow. Mass-choked and combustion-choked flows have remarkable similarities. Figure 8b and Figure 7b show a detailed view of the pressure fluctuations over a time interval of 20 ms. The fluctuations in the two cases have same frequency and propagation speeds within the uncertainty limits of the method used to compute them.

B.1. Isolator Shock Dynamics Visualization

The flow configuration in the isolator can be visualized using the plasma natural luminosity as shown in Figure 9. The images show six different stages of the isolator flow, in a typical case with inlet unstart caused by combustion heat release. When fuel injection is initiated, the backpressure generated by the jet-crossflow interaction separates the boundary layer, creating a shock-train in the isolator (Figure 9a-i). If the interaction is particularly strong, like in this case, the shock-train extends upstream covering almost the entire length of the isolator (Figure 9a-ii). At this stage, the boundary layer is separated by the leading shock but is able to reattach immediately downstream. A new separation probably occurs at the impingement point of the second shock. When the flow in the combustor chokes and the pseudo-shock propagates to the injectors, the isolator backpressure is further increased, and the boundary layer separates completely. At this point the images show large flow recirculation near the wall (Figure 9a-iii), with turbulent structures convected periodically back and forth in both longitudinal and azimuthal directions. During this phase, flames can be observed to propagate into the isolator through the separated region as in Figure 9a-iv.

The longitudinal periodic migration of the gas in the separated region intensifies and, interacting more effectively with the supersonic core, ultimately breaks down into a series of self-sustained oscillations. The shock-train transitions from x-type to λ-type as shown in Figure 9a-v. The low speed region downstream the Mach disc, having higher density and temperature, appears brighter in the images. The shock-train in Figure 9a-v has a total of five shocks with decreasing size and spacing. This configuration corresponds to the phase of maximum stretching of the shock-train. During the oscillations, the distance between the shocks is reduced until the entire shock-train nearly collapses to a single normal shock (Figure 9a-vi). Depending on the amount of fuel injected, the shock-train can either keep oscillating around a fixed location in the isolator or propagate up to the inlet causing unstart. With unstarted inlet, the flow assumes the configuration of Figure 9a-vii, characterized by a spatially uniform luminosity with fluctuating intensity at a frequency of ~400 Hz. These fluctuations are most likely associated with the pressure waves travelling through the isolator in unstarted conditions, as described in Sec. III.B. Despite the nature of these phenomenon is still unclear, inlet buzz seems the most probable explanation. The same qualitative behavior was observed also for the non-reacting case. This result is in agreement with the pressure comparison of Figure 8 and Figure 7.

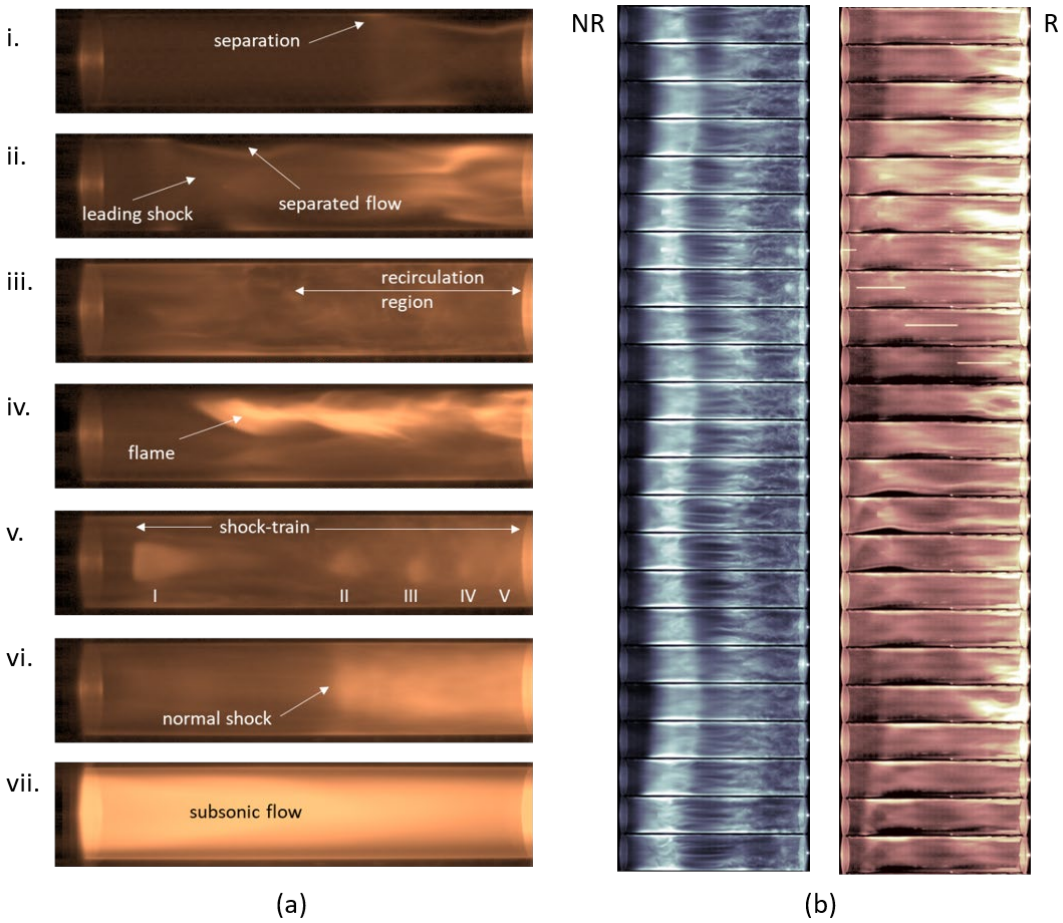

Figure 9. Average pressure distribution in the isolator with choked combustor. Comparison between choking induced by mass injection (blue) and by combustion (red). Flow direction is from left to right.

Figure 9b shows isolator imaging during the propagation of the pseudo-shock, for both reacting and non-reacting conditions. The objective is to verify if the different shock propagation dynamics in the combustor has an impact on the isolator shock-train behavior. The sequences of Figure 9b are taken at 10 kHz in the same nominal conditions as Figure 6. They span a total time of 2.4 ms during which the pseudo-shock is propagating through the combustor. Under these conditions the shock-train is in the configuration of Figure 9b, with a strong x-type leading shock positioned in the front part of the isolator. The images show that the dynamics of the shock-train is very similar in the two cases. The shock-train undergoes small oscillations (less than a diameter in amplitude) with a frequency of 1250 Hz. This similarity suggests therefore that, at least at this stage, the characteristics of the pseudo-shock propagation are not affecting significantly the isolator dynamics that is dominated by shock-boundary layer interaction.

B.2. Combustor Shock Propagation

The post-choking propagation of the pseudo-shock in the constant area combustor was studied by plasma luminosity imaging at 20 kHz. Figure 10 shows an example of the pseudo-shock visualization for both non-reacting Figure 10a) and reacting (Figure 10b) cases.

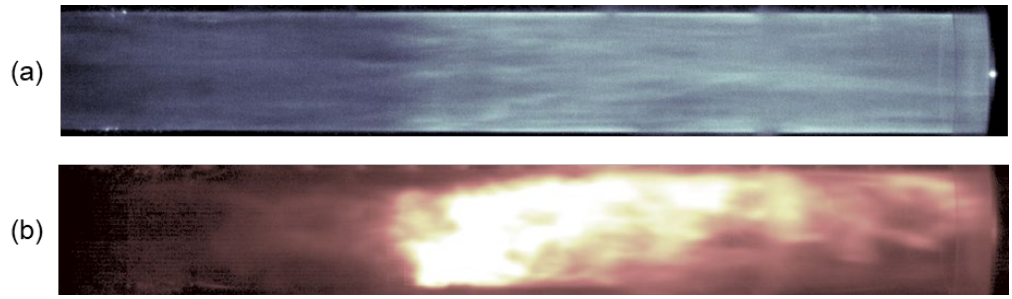

Figure 10. Pseudoshock visualization in constant area combustor for a) non-reacting and b) reacting cases.

In the non-reacting case, all the radiation is produced by the hot plasma. Upstream of the pseudo-shock it is possible to notice the development of the air jets from the injectors, running streamwise along the wall. The pseudo-shock appears as an intensification of the brightness due to the density rise caused by the shocks. In the reacting case, the light intensity is much larger and partially saturated the camera. At this intensity scale the plasma luminosity is almost invisible and most of the light results from OH^* and CH* chemiluminescence. Upstream it is possible to distinguish the head of the shock-train followed by the dissipative region, where a combination of lower speed and high temperature accelerates the combustion process and the production of combustion radicals. Figure 10a shows a comparison between the propagation of the pseudo-shock in the non-reacting and the reacting case. Each sequence is composed of 51 images equally spaced in time for a total duration of 12.5 ms. In the non-reacting case (NR), choking was induced injecting a mass flow of air equal to 34% of the inlet mass fraction, whereas in the reacting case (R) ethylene was injected at an overall equivalence ratio ϕ=2.0. These two cases were selected for comparison because they have similar propagation time through the combustor. From the images, it is evident that in the non-reacting case the shock propagation is regular with nearly uniform velocity, whereas in the reactive case the shock follows a more complicated pattern.

Setting a threshold on the image intensity it was possible to quantify the shock position as function of time, as shown in Figure 11b, and compute the propagation speed by differentiation (Figure 11c). Both cases have a similar average speed, -20.8 m/s for the non-reacting and -17.3 m/s for the reacting but the standard deviations are 8 m/s and 41 m/s respectively. Furthermore, the propagation speed in the reacting case alternates positive peaks (as high as 66.3 m/s) and negative peaks (as high as -113.1 m/s) with an average frequency of 555 Hz. The velocities shown in Figure 11c are absolute, i.e. computed in the laboratory frame. Therefore, they are the combination of the flow velocity and the shock speed relative to the flow. Anyway, since the pressure measurements did not reveal any significant fluctuation upstream of the pseudo-shock, the flow speed is expected to be nearly constant in the combustor, and the velocity variations in the reactive case would be actual variations of the shock speed. Similar to the observations made about the direct-connect combustor, combustion heat release is expected to have a prominent role on the irregular propagation of the pseudo-shock, making the prediction and analysis of the choking process much more difficult. The irregular pseudoshock propagation can be attributed to combustion instability and was identified as an issue that should be addressed in a realistic dual-mode scramjet design operating in the takeover regime.

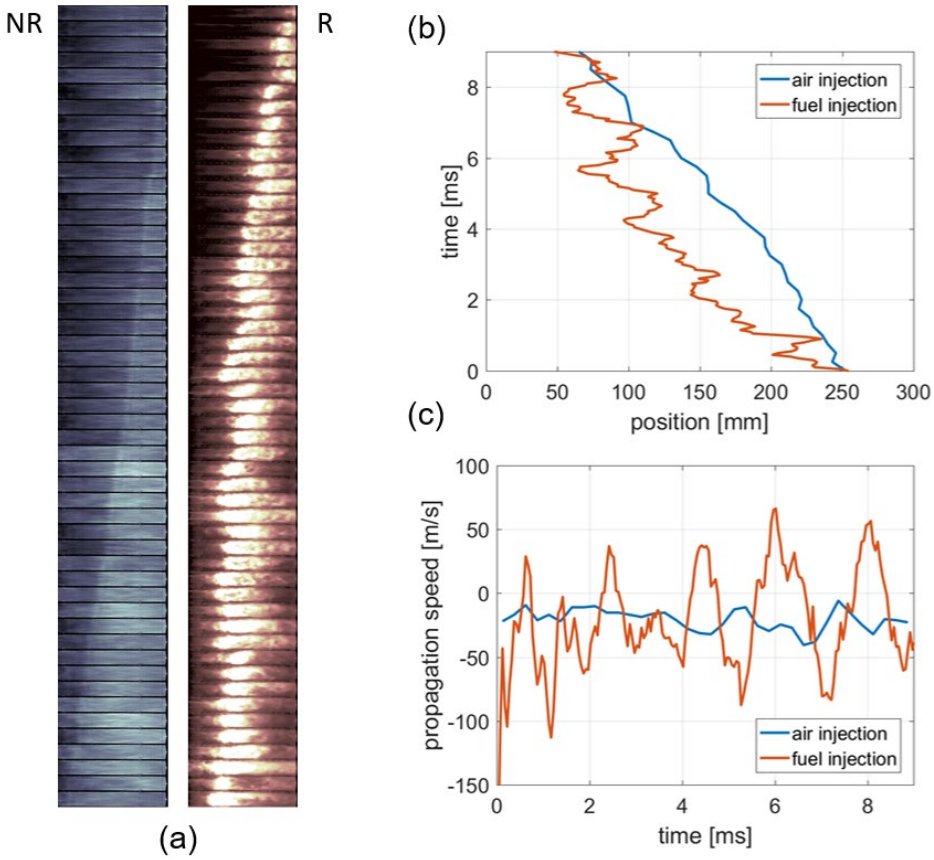

Figure 11. Average pressure distribution in the isolator with choked combustor. Comparison between choking induced by mass injection (blue) and by combustion (red). Flow direction is from left to right.

C. Scramjet Design

For a scramjet operating safely and efficiently near mode transition and unstart, several performance criteria must be met. Principal among these is combustion stability and the need for more complete detection and control of transition and potential unstart mitigation. Figure 12 lists the parameters needed to be considered in scramjet design, which include the fuel injection to supersonic core, cavity flameholding arrangement, and the area relief to accommodate the combustion heat release. The cavity flameholder reduces the combustion induction time and improves the overall flow mixing. Proper combustor area relief is necessary to optimize the combustion heat addition process and stabilize the flame downstream of the cavity flameholder, i.e., to maximize the combustion efficiency to obtain the potential performance of scramjet engines. Billig [9] defined

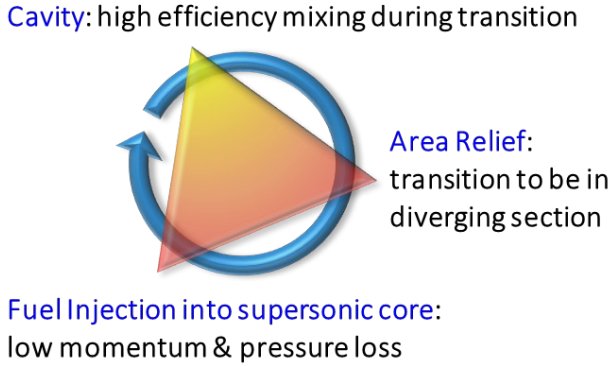

Figure 12. Parameters considered in scramjet design.

the optimal heat addition process in scramjet combustor based on pressure-area relationship, i.e., the least entropy rise for a give stagnation temperature rise and set of initial conditions, which can be realized for the case of sonic condition at combustor exit. The combustion efficiency can be enhanced by improving the fuel-air mixing rate, flow residence time, static pressure/temperature of supersonic flows in the combustor that decrease the Mach number along the flowpath in supersonic flow regime.

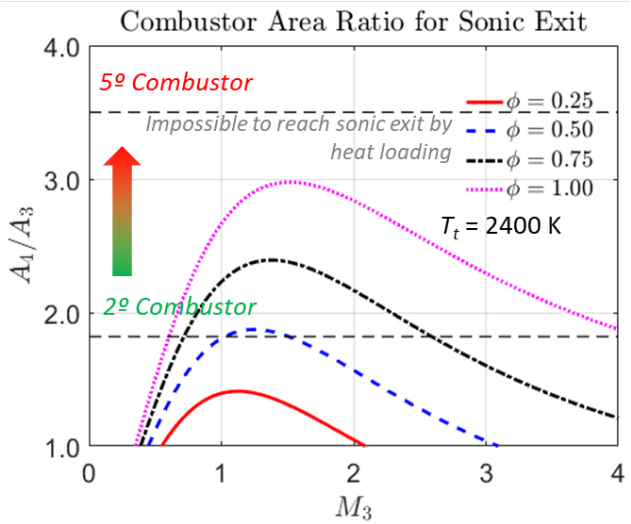

Figure 13. Scramjet operational diagram with the sonic condition at combustor exit.

Combustor performance analysis shown in Figure 13 indicates that there exists no solution for the 5-deg combustor to choke at the combustor exit at any given combustor entry Mach number and ideal combustion heat addition rate at equivalent fully premixed equivalence ratio. Theoretically, the 5-deg combustor with current length cannot be choked by combustion heat loading at current flow total enthalpy condition. The experimental observation confirms the theoretical prediction and evidences the potential choking location for scramjet combustor with cavity flameholding and excessive area relief, i.e., the cavity region. In addition, the diverging combustor with excessive area relief tends to have fast Mach number increase and static temperature/pressure drop along a short flowpath, which will potentially quench or freeze the ongoing high-temperature combustion reactions.

The combustion in 2-deg combustor is more efficient than that in 5-deg combustor in this study. As shown in Figure 14, the 2-deg diverging combustor choking at a smaller ϕ compared to the 5-deg diverging combustor. Interestingly, the 5-deg combustor does not choke at its peak combustion heat addition into the supersonic flow but at extremely impractical high fuel loading when its combustion efficiency and heat addition into the core flow are low.

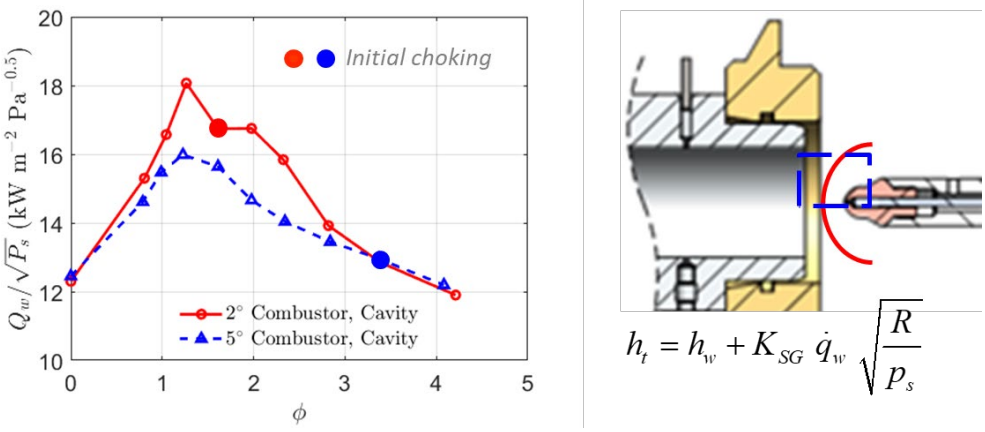

Figure 14. Normalized heat flux measurements with 2-deg and 5-deg diverging combustors.

Intense flame chemiluminescence indicates the initial choking location as shown in **Figure 15**, the choking occurs in the diverging combustor section and propagates upstream until the cavity flameholder in the 2-deg combustor, while the choking occurs inside the cavity region (close to the ramp side) and no flame propagation is observed in the 5-deg combustor. Therefore, the choking event and unsteady flame propagation in 2-deg combustor are mainly induced by excessive heat addition into the core flow as indicated by the heat flux measurement; in contrast, the choking event in 5-deg combustor mainly results from excessive total pressure losses from extremely strong jet-induced bow shockwaves and recompression shock at cavity ramp, which decreases the Mach number in the supersonic core inside the cavity region, rather than combustion heat addition in the diverging section.

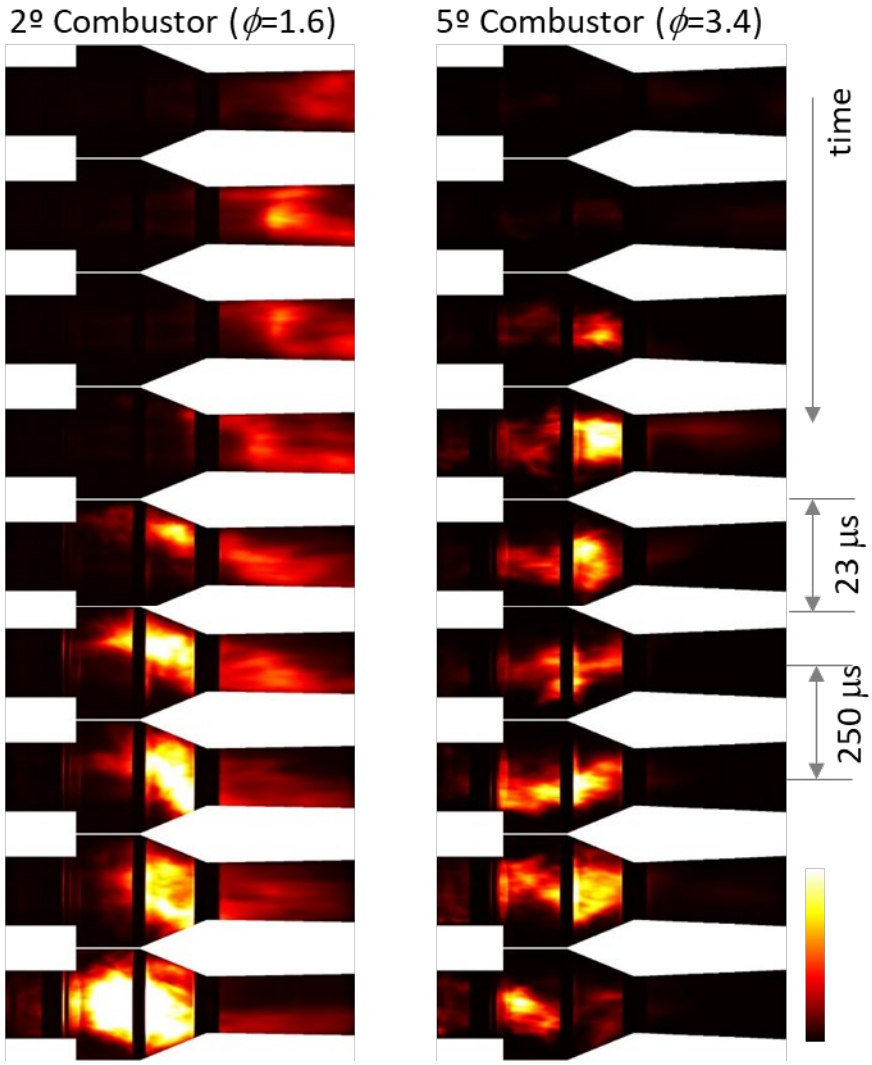

Figure 15. High-speed flame chemiluminescence at choking limit.

Given the same fuel mass flow rate below the choking limit and flow conditions at the isolator exit (i.e., combustor entry), the Mach number at combustor exit is much higher than one for the 5-deg combustor than that for 2-deg combustor, i.e., the combustion process in the 2-deg combustor with a cavity flameholder is closer to the optimal process. It is noteworthy that the

unsteady flow dynamics occurring in the cavity and diverging combustor section results from the pseudo shock dynamics during the inlet-isolator-combustor interaction.

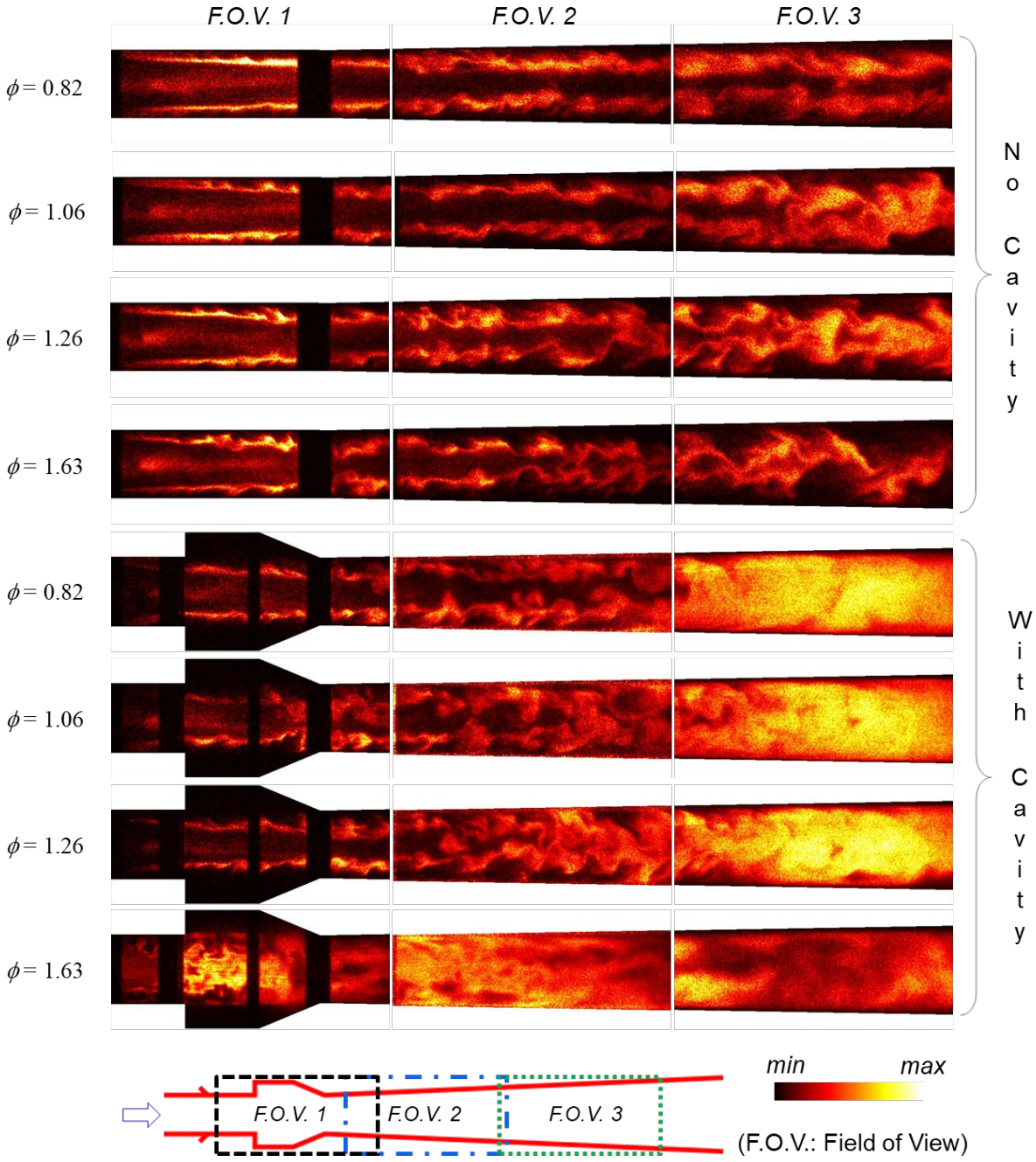

Figure 16. OH-PLIF images of steady-state flames in 2-deg diverging combustor.

Resolving detail flame structures and distributions are necessary to further understand the cavity influences on combustion dynamics although the cavity enhances the overall combustion and impacts the combustor performance as quantified by static pressure measurement on the combustor wall, total pressure and heat flux measurements at the combustor exit. Figure 16 shows the flame structures at steady state are resolved using OH PLIF imaging in three fields of views (F.O.V.) with/without a cavity flameholder at various ethylene fueling rates.

It is observed that the cavity promotes the transition of laminar-like flame fronts to large-scale flame structures and direct the fuel into the core of the flow in the diverging combustor. Without a cavity flameholder, a laminar flame structure is sustained over a longer distance in the constant area combustor downstream of the fuel injection before the transition to large-scale turbulent flames. The increased ethylene fueling rate promotes the flame front transition process inside the constant-area section. With the presence of a cavity, the flame fronts are perturbed immediately from the cavity leading edge due to expansion waves and shockwaves introduced by the cavity. The fuel-air mixing near/above the shear layer originating from the cavity leading edge is further enhanced by the shear layer instability and the shockwave-shear layer interactions. At the cavity trailing edge, a recompression shockwave developed above the cavity ramp deflects the fuel-air mixtures/shear layer toward the core of the flow, which cannot be observed in the configuration without a cavity. The large-scale flame structures enhance the fuel-air mixing processes by entraining massive oxidizers into fuels, stretching fuel-air interfaces, increasing the interfacial areas, and/or steepening the local concentration gradients in molecular diffusion processes [52]. As shown in Figure 16, the hydroxyl radicals indicating the ongoing high-temperature combustion reactions fill the combustor core in the most downstream field of view at ϕ = 1.26 without a cavity. In contrast, the intense combustion spreads over the entire combustor volume downstream even at fuel lean condition ϕ = 0.82 with a cavity in this study. These observations are consistent with the quantitative measurements using pressure transducers and heat flux probe.

The axisymmetric scramjet with a cavity flameholder and a diverging combustor (cone angle 2 deg) is experimentally investigated with: (1) no fueling, (2) air injection and (3) ethylene injection at various fueling rates. Parallel experiments are carried out at the same fueling schemes with the cavity flameholder replaced by a constant cross-section tube. Figure 17 presents the pressure distributions along the flowpath downstream of the fuel injection port in scramjet combustor configurations with and without a cavity flameholder.

The combustion stabilization in a generic 2-deg diverging combustor configuration has been achieved by the cavity flameholder as indicated by comparisons between the pressure distributions with and without a cavity. With an axisymmetric cavity flameholder, the pressure profiles have a peak (local maxima) in the cavity ramp region and another peak in the diverging combustor region. The first pressure peak at the cavity ramp results from the shear layer impingement on the cavity ramp while the second peak originates from the combustion heat addition. In supersonic flows, the combustion heat addition decreases the flow Mach number while the area relief increases the flow Mach number; whether the Mach number decreases or increases depending on the combined effects from the combustion heat addition rate and the combustor area relief. The static pressure increases with the decreasing Mach number along with the flow path. The ordinary differential equation of the static pressure without the wall friction term for constant specific heat and molecular weight term from Shapiro [53] is

$$\frac{dP}{P} = \frac{\gamma M^2}{1-M^2}\left[\frac{dA}{A} - \left(1+\frac{\gamma-1}{2}M^2\right)\frac{dT_t}{T_t}\right].$$

where P is the static pressure, M is the Mach number, A is the combustor cross-section area, and T_t is the flow total temperature. For $M>1$, the combustion heat addition dominating the process leads to $dP/P>0$, *i.e.*, $\left[1+(\gamma-1)M^2/2\right]dT_t/T_t > dA/A$, as evidenced by the pressure

distribution shown at x = 450-600 mm in Figure 17 a) and)b with overall equivalence ratio ϕ=1.26. The local maximum pressure value increases with the fueling rate (ϕ=0.81-1.26) results from the increased combustion heat addition while the combustor geometry is unchanged. Downstream of the local pressure maxima in the diverging combustor, most of the injected fuel has been consumed in combustion and the combustor area relief dominates the aerodynamic process. The area expansion increases the flow Mach number in the supersonic core and decreases the static pressure along the flowpath. The combustor downstream of the maximum pressure location behaves as an expansion section at x > 650 mm. In contrast, these phenomena are not observed in the combustion configuration without a cavity flameholder shown in Figure 17 c) and d). The cavity flameholder can enhance the supersonic combustor performance by promoting the fuel-air mixing, enhancing heat transfer rate from the boundary flow region to the supersonic core, and reducing the combustion induction time by flow preheating and potential radical supply to flow downstream from flow recirculation region in the cavity. Due to the lack of such mechanisms for combustion enhancement in flow configuration without a cavity, the combustion heat addition in the diverging combustor is not sufficient to compete with the area relief effect, which results in the continuous pressure drop along the flowpath. In addition, the pressure distributions are not sensitive to the fuel mass flow rate due to the insufficient fuel-air mixing as shown in Figure 17 c).

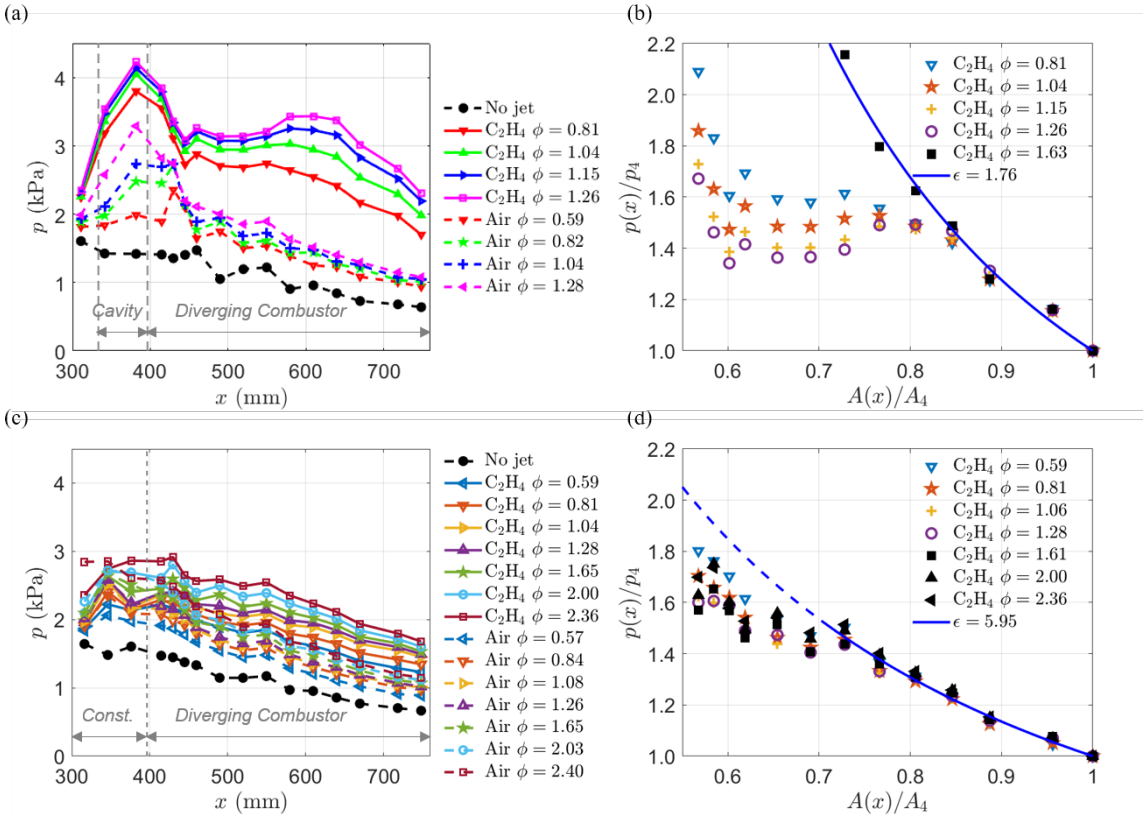

Figure 17. Pressure distributions in a model scramjet with a),b) a cavity flameholder, and c),d) without a cavity flameholder.

As the aerodynamic parameters of supersonic core flow in the diverging combustor determine the critical operating condition leading to the flow choking and scramjet operational mode transition, quantitative heat flux and total pressure measurements are conducted in the

supersonic core flow at the combustor exit to assess the combustor performance enhanced by the cavity flameholder.

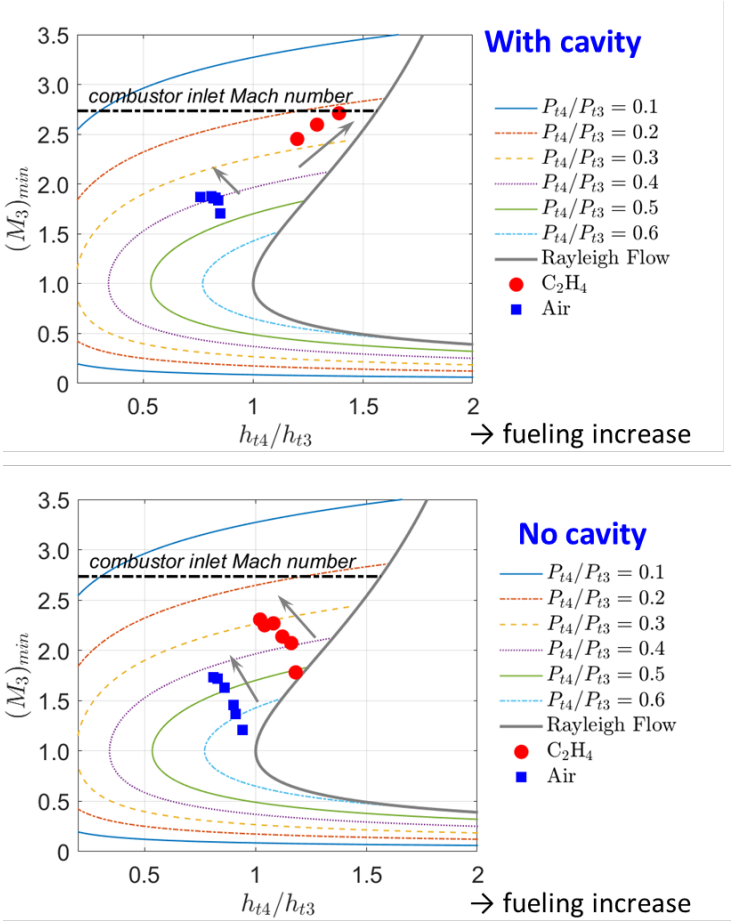

Figure 18. Heat flux measurements at core flow stagnation point downstream of combustor

Figure 18 shows the heat flux measurements at the stagnant point after a normal shock in various ethylene fueling rates. The normalized heat flux is linearly related to the total flow enthalpy and hence an explicit indicator of the combustion heat addition. It is clearly observed that the pressure rises in the diverging combustor result from the combustion heat release. With the cavity, the normalized heat flux increases by 50% with the increase of the fueling rate until the flow is choked at $\phi = 1.6$ and above. With the air injection, the total flow enthalpy decreases with the air mass flow rate due to the cooling effect of the room-temperature air. The normalized heat flux with air injection is approximately half of that with ethylene injection at equivalent $\phi = 1.3$. Interestingly, the cooling effect from air injection is more apparent with a cavity flameholder compared to that without a cavity. As the cavity enhances the injectant-freestream mixing, the heat transfer from the supersonic core to the cold injectant is more efficient and the flow enthalpy in the core flow is lower.

Figure 19 shows the typical scramjet operation mode transition from the dual-mode scram to the ram mode, which corresponding to the descending phase of hypersonic flight. The pressure measurements are conducted in the model scramjet with a 2-deg diverging combustor. The scramjet transition can be divided into three phases, i.e., the flame propagation phase, ram-mode phase and the unstart phase. In a typical test, the fuel is injected at the time of 0.26 s and the fuel mass flow reaches to its maximum and steady condition at 0.33 s. With the increasing of ethylene fueling rate below the choking limit, the combustion stabilizes inside the diverging combustor as indicated by the high-pressure region in the pressure contour. Pseudo shocks develop once the flow is choked by excessive heat release and the unsteady shockwaves propagate upstream until the cavity flameholder region. The flame and shock propagation in this phase are highly unstable. Once the flame propagates into the cavity, the strong combustion and flow blockage introduce back pressure that is sufficient high to separate the flow inside the isolator, as indicated by the

high-pressure region in the pressure contour upstream of the cavity zone. The isolator is sufficient long to accommodate the pseudo shocks only during the 0.32-0.36 s. Around the 0.36 s, the pseudo shock is close to the scramjet inlet and the unsteady boundary layer separation starts to interact with the inlet. The unsteady flow dynamics drive the pseudo shock further upstream until a bow shock develops upstream of the inlet, which is called scramjet unstart. Once this bow shock develops, the flow compressed by the shock is spilled and the incoming mass flow rate is decreased. The combustion may exist inside the isolator region due to the reverse flow during an unstart event. As the incoming oxygen mass flow rate is decreased and the fuel mass flow rate is constant, the combustion intensity decreases at this time frame and results in lower flow blockage and weaker back pressure rise. The standing normal shock will be swallowed by the inlet and the air mass flow rate entering the scramjet engine increases. The combustion will recover due to the increased oxygen supply upstream. Once again, the increased combustion introduces strong heat release and choke the flow again. This entire process is cyclical, as indicated by the intense periodic oscillation over the entire internal flow channel of the scramjet model. Therefore, the flow oscillation is the totality of the scramjet inlet-isolator-combustor interactions. Further investigation on the flame dynamics during the unstart processes needs to be fully resolved and the strategy for unstart control needs to be proposed.

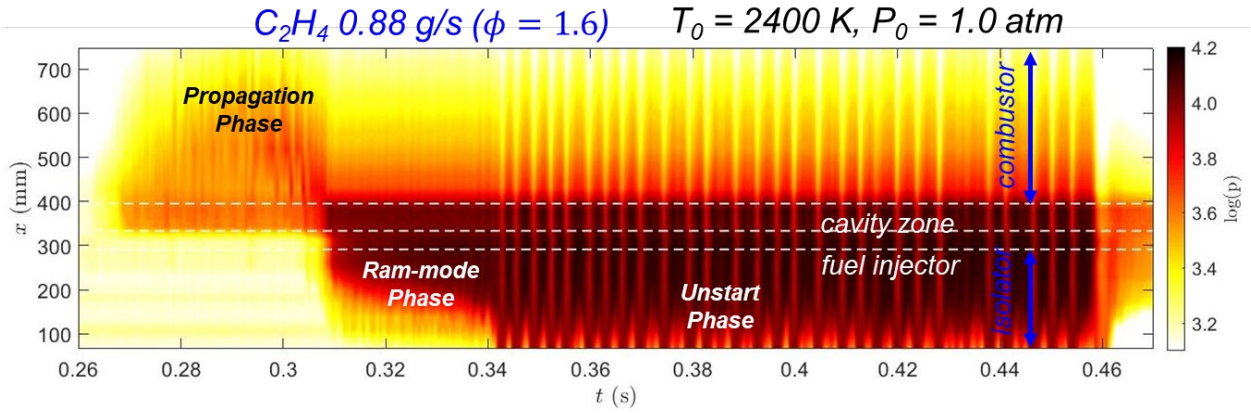

Figure 19. Pressure contour in the x-t plane during the scramjet dual-mode transition process.

B.3. Comparison Between Axisymmetric and Perisymmetric Flowpaths

In this section, the comparison of flow dynamics in scramjet models with axisymmetric and perisymmetric cross-sectional shapes is presented. Figure 20 depicts the cross-sectional shape of the perisymmetric scramjet model. The perisymmetric cross-section incorporates 2 walls with constant curvature which forms the sharp corners around the joint at the top and bottom. The perisymmetric shape is inspired to improve the fuel penetration and mixing into the core flow, which is one of the issues associated with the axisysmmetric scramjets. Figure 21 shows an overview of axisymmetric and perisymmetric scramjet models. Both models have an inlet with CR=1.9, an isolator of 200 mm in length, a combustor of 300 mm in length. The isolator of the perisymmetric model is instrumented with the pressure transducers on the top and middle lines to quantify the spatial distribution of the wall pressure. Table 2 summarizes the freestream conditions used for the comparison.

Table 2. High Enthalpy Test Conditions (Axi vs Peri)

Freestream			
Stagnation Temperature	T_{t0}	2540	K
Stagnation Pressure	P_{t0}	220	kPa
Mach Number	M_1	4.48	-
Static Temperature	T_1	503	K
Static Pressure	P_1	760	Pa
Density	ρ_1	0.053	kg/m^3
Velocity	V_1	2023	m/s

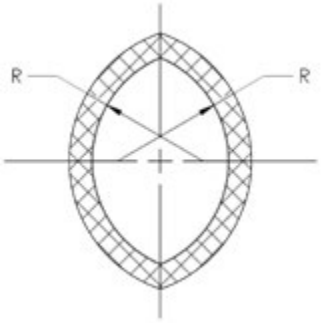

Figure 22. Schematic of the perisymmetric cross-section.

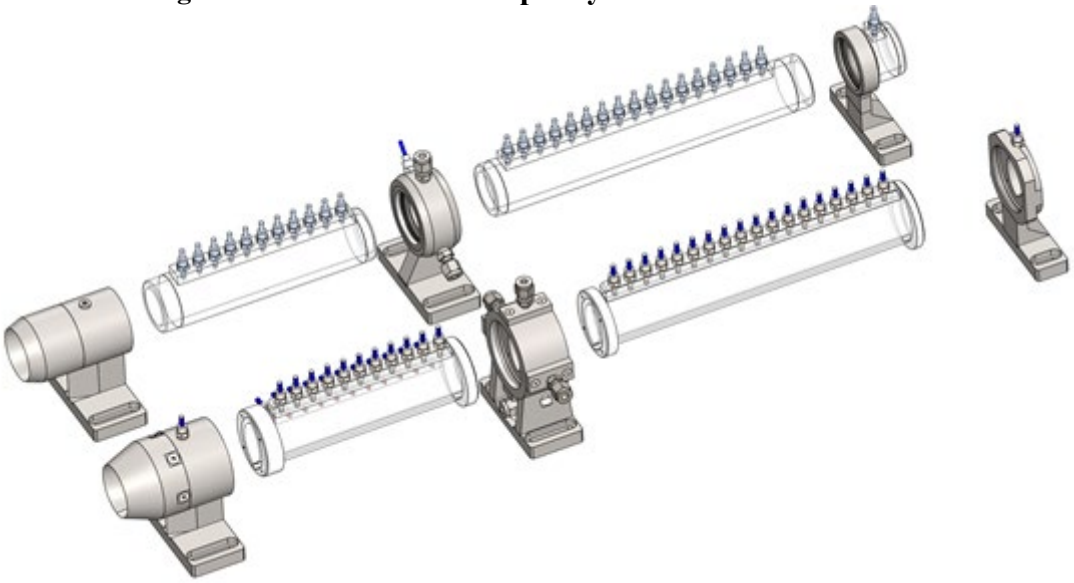

Figure 23. An overview of the axisymmetric (top) and perisymmetric (bottom) scramjet models.

Figure 24 shows the averaged wall pressure data measured for the axisymmetric and perisymmetric scramjet models. For the axisysmmetric model, the pressure in the isolator is not

disturbed at $\phi < 1.63$. However, an increase in ϕ to 1.69 creates the pressure disturbance traveling into the isolator. It is assumed that this pressure rise attributes to the pseudoshock located in the isolator. At $\phi > 1.69$, monotonic decreases of the pressure in the combustor is clearly observed, which indicates the presence of thermal throat and the subsonic acceleration towards downstream (ramjet mode). The pseudoshock is located more upstream as the value of ϕ increases, resulting in the rise of the isolator pressure. It is believed that the inlet is still started at $\phi = 2.02$ because of the monotonic pressure increase in the isolator. Similar to the axisymmetric model, the isolator pressure of the perisymmetric model is not disturbed at $\phi < 1.47$. However, the pressure measured at the combustor entrance is 16.1 kPa at ϕ = 1.47 which is 121 % higher than that of the axisymmetric model measured at ϕ = 1.46. In addition, the pressure in the combustor of the perisymmetric model exhibits a monotonic decrease at $\phi = 1.47$. Therefore, it is suggested that the more intense combustion happens in the combustor of the perisymmertic model due to the enhanced fuel penetration and mixing. The isolator pressure of the perisymmetric model finally reaches the high-pressure value at $\phi = 1.91$, indicating the occurrence of inlet unstart.

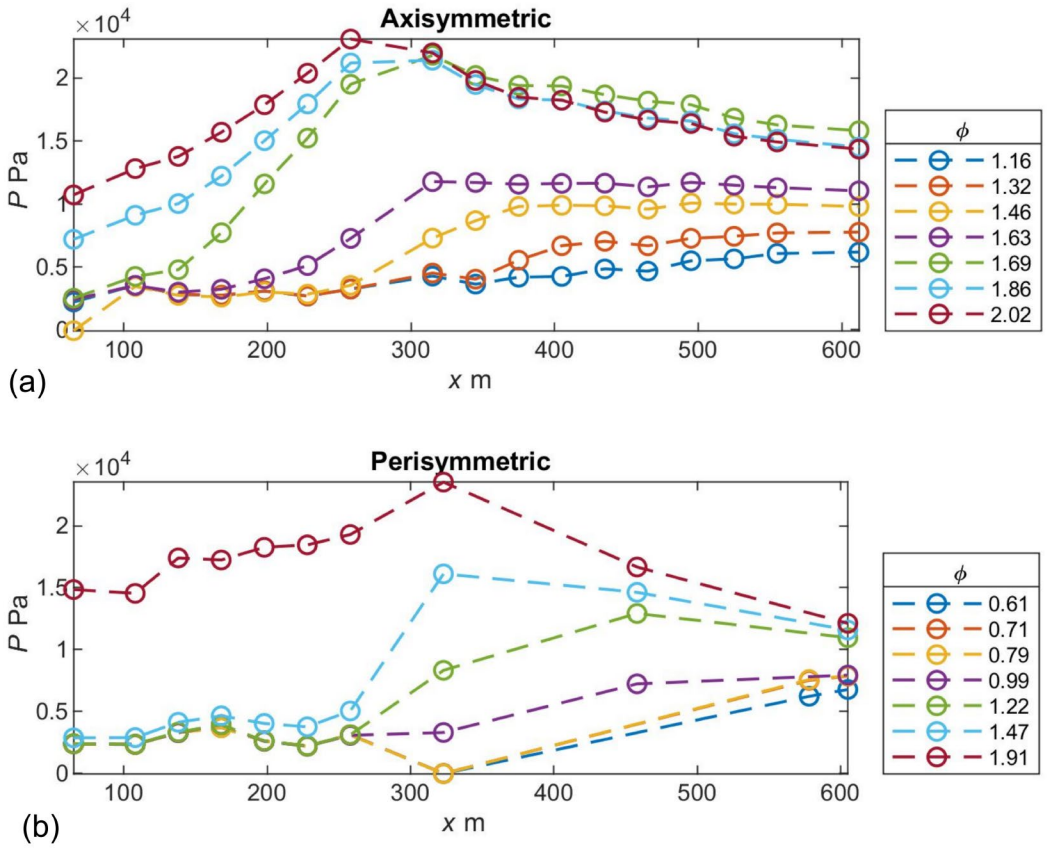

Figure 25. Averaged wall pressure data for (a) axisymmetric and (b) perisymmetric scramjet models.

5. NCSU Contribution

A. Overall objectives and goals

The contribution of NCSU team is to analyze UIUC data to unravel the fundamentals of unstart initiation and propagation from the perspective of flow physics. Through the analysis, the following questions are examined to elucidate the flow physics associated with unstart initiation:

- For the 2D axisymmetric test article considered, does the boundary layer separate prior to unstart initiation?
- If yes, where would the separation most likely occur?
- If yes, at what conditions does the flow separation most likely to occur (e.g., in scram mode, ram/scram transition, ramjet, etc.)
- Can flow separation occur in started operation?

The other aspect of the analysis deals with the flow interactions that facilitate the propagation and drive the pseudoshock dynamics during its propagation. The following questions are addressed:

- For the 2D axisymmetric test article considered, what is the contribution of turbulent combustion on the dynamics of the unstart propagation?
- Through what mechanisms do the isolator pseudoshock train and combustor dynamics get coupled during unstart and how do they impact the pseudoshock dynamics during propagation?

The final aspect of the NCSU contribution relates to the development of high-speed pressure imaging to study the unstart event, which could be employed to track the initiation and propagation of the unstart. This tool will be extended to high-enthalpy flow applications and will be used to image the unstart event in a time-resolved manner.

B. Data available and Approach outline

The following data is available from a series of experiments performed at UIUC on a 2D axisymmetric inlet/isolator test article prior to and during an unstart event:

- Simultaneous pressure in isolator and flow luminosity within isolator
- Simultaneous pressure in combustor and flame luminosity within combustor
- Non-synchronized but simultaneous pressure in isolator and flame luminosity in combustor

With these datasets, the elements of analysis that was performed varied for different study objectives. For the analysis that involved unraveling the physics of unstart initiation included:

- Obtain the pressure profiles at various operation modes and prior to unstart initiation (as close to initiation as possible)
- Analyze if the thermal choke pressure responds to the upstream and downstream oscillations of the combustion zone, which can in turn impact the unstart onset pressure;
- Perform stream-thrust averaged computations following Shapiro and Smart as well as 2D RANS to match the experimental pressure profiles (ongoing)
- Once matched, investigate the computations predict a mean flow separation for the given pressure profiles (ongoing)

For the analysis to unravel the isolator/combustor coupling, the analysis procedure comprised

- Compare the pressure oscillation and pseudoshock oscillation amplitudes with mass addition and combustion induced unstart to unravel the impact of combustion oscillations on pseudoshock dynamics
- Analyze the origins of the pseudoshock oscillations by comparing the power spectra of isolator pressure fluctuations and pseudoshock oscillations before and during unstart and unstart induced by mass addition and combustion.

The following provides highlights of the main findings of the effort. Since the analysis on the inlet unstart initiation is ongoing, only the isolator/combustor coupling mechanisms are highlighted n this report.

C. Details of isolator/combustor coupling mechanisms

First, we did an elimination procedure to see if the oscillations frequency are fed by the flowfield and geometry or inherent thermoacoustic oscillations. To this end, we obtained the pressure oscillations within the combustor for the cases without combustion (examining base flowfield/geometry), with combustion but without unstart getting as close to unstart limit as possible (examining inherent thermoacoustic oscillations) and combustion with unstart (examining the coupling between isolator shock train with combustion unsteadiness). Figure 26 shows the power spectral density of wall pressure fluctuations at a representative location within the combustor (all other locations have the same PSD signature). It can be seen that no discernable peaks occur at isolator shock oscillation frequencies in both baseline flowfield and combustion without unstart case allowing us to eliminate flowfield and baseline thermoacoustics as the causative mechanisms for unstart shock oscillations. We do see a clear peak in the combustor pressure oscillations at 400 Hz (subharmonic of unstart shock oscillations) when we have an unstart event. So, the question is what mechanisms within the isolator/combustor coupling cause this to happen.

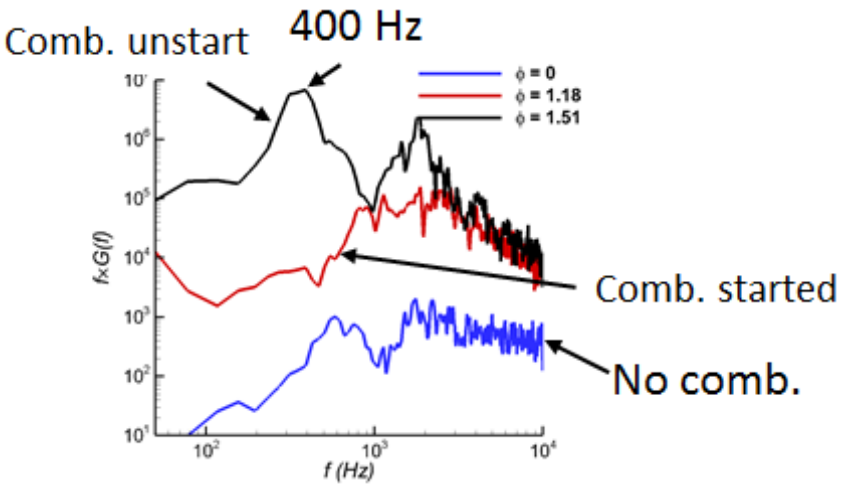

Figure 26: Wall pressure fluctuation PSD inside the combustor for three situations: no combustion, combustion without unstart and combustion with unstart

To examine the isolator/combustor coupling, we examined the mass addition driven unstart case where the flow blockage was maintained constant during unstart. In other words, there is no feedback of pressure fluctuations into the isolator due mass addition. We present one representative case of mass addition strength where the shock goes through a full unstart beginning from the started inlet, going through highly oscillatory unstart shock motions, followed by full unstart with subsonic flow within the entire isolator. Figure 27 shows the wall pressure time trace measured inside the combustor, one station close to the cavity flame holder and other close to the tail end of the combustor, along with the corresponding shock position within the isolator. Summarily, we observe that during the oscillatory unstart shock oscillatory phase, there are corresponding large pressure fluctuations in the combustor section that are especially strong at the combustor beginning (near to the cavity flame holder). The change in the pressure in the location closest to cavity where the ram-mode combustion happen can be up to 30%. *In other words, the shock oscillations within the isolator cause pressure oscillations on the order of 30% in the locations where combustion occurs.* In the combustion situation, this pressure oscillation magnitude is sufficient to modulate the combustion behavior and heat release rate to establish feedback.

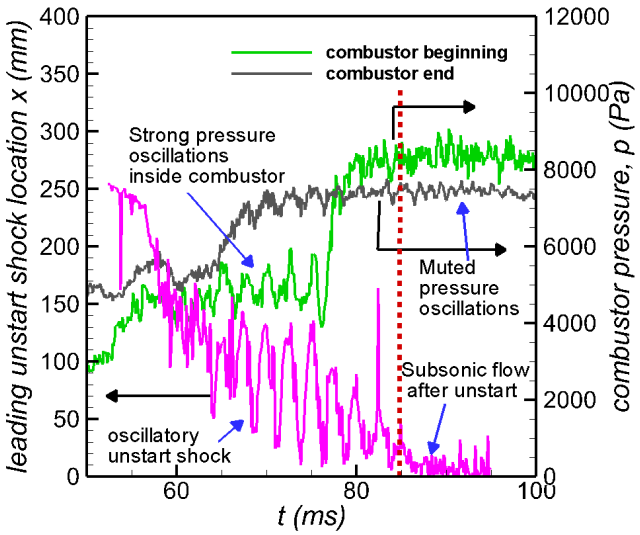

Figure 27: Wall pressure time trace inside the combustor during after unstart and the corresponding unstart shock trajectory

In the specific case of heat addition another mechanism may be active. The upstream shock motion will result in an increased heat addition required for choking, $\dot{Q}^*$, per Laurence et al. (2013). This causes the sonic throat to shift downstream in the combustor for the same heat addition rate, and in turn causes the unstart shock to move downstream. The situation is reversed with the downstream shock motion and the sonic throat quickly moves considerably upstream causing the unstart shock to propagate upstream. This feedback loop is further enhanced by the heat addition changes due to pressure modulations as the unstart shock train oscillates within the isolator. At this point we do not have a measure of exact sonic throat location to validate this postulate; however, the time series of intense combustion location provide a qualitative consistency of this hypothesis.

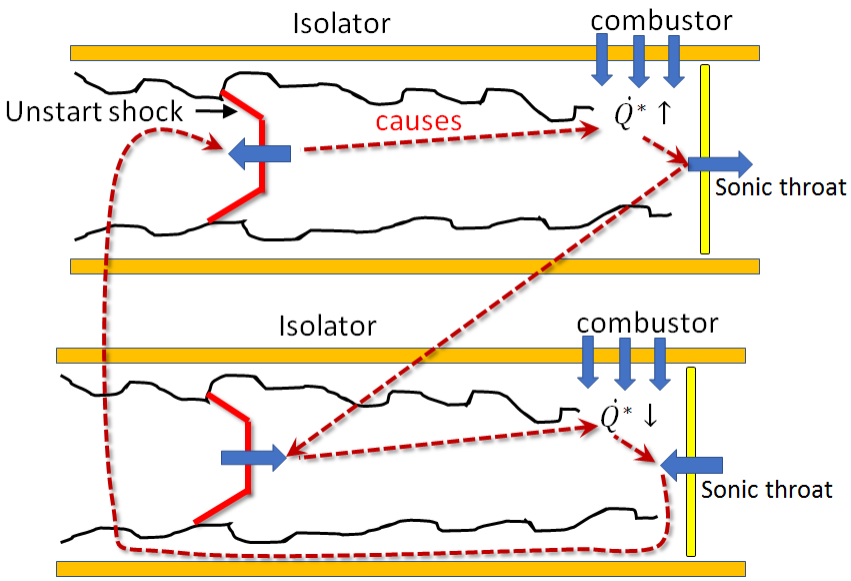

Figure 28: Illustration of the isolator/combustor coupling mechanism to explain the unstart shock oscillations

Hence, we believe that the oscillatory nature of unstart with combustion is caused by a feedback loop between the unstart shock and sonic throat oscillations with additional contributions from heat release and the corresponding back pressure changes. It should be noted that this is a rudimentary picture and in the near future, we will get to the details and nuances to validate and enhance this postulate. We are also analyzing the unstart pressure data to uncover the existence of nodes downstream of the leading shock leg that form critical locations to coupling the isolator and combustion pressure fluctuations.

The final question is if the 800 Hz isolator shock train oscillations is what one would expect to happen. To examine this, we note that there is a Mach disk in the center core when the leading unstart shock legs intersect, as seen in the black region of the figure. Hence, we establish a subsonic core as well as a subsonic separated flow region that extends through the isolator and into the combustor where the flow reaches Mach 1 due to combustion or simply due to mixing. A representative length scale of the subsonic region is between isolator mid-length through middle of combustor where the sonic throat is typically formed during ramjet operation. We use the resonant frequency expression following Newsome (1984) that provides an estimate of the dominant acoustic oscillation frequency.

$$f = \frac{\bar{a}}{2L}(1 - M_{NS})(1 + M)$$

Using normal shock relations to obtain M_{NS} and the estimate of the freestream speed of sound, we observe the shock oscillation frequency should be about 1300 Hz. It should be noted that this is a first order estimate and exact values of many of the variables in the above equation are approximate. Despite this, the proximity of the predicted and observed shock oscillation values indeed suggest that the shock oscillations are driven by acoustic resonance to begin and is subsequently coupled to the sonic throat oscillations through the feedback loop.

6. FUTURE PLANS

In futures years, we hope to advance our study to investigate novel Flowpath geometries bridging fundamental studies on scramjet choking and unstart and realistic scramjets. Such geometries will be inspired by and derived from practical applications of scramjets, with the aim of optimizing the performance of scramjets beyond that offered by simpler, more canonical geometries. Tests similar to those conducted on axisymmetric and rectangular geometries will be conducted to characterize the internal flow during incipient choking and choked conditions. An effort to compare cases solved using 1D choked flow models to experimental results in axisymmetric and higher dimensional geometries will be undertaken to validate predictive tools for unstart threshold and choking location in addition to revealing the effects of higher dimensional flow on the choking process.

7. PERSONNEL SUPPORTED

Faculty

Professor Tonghun Lee (UIUC)

Professor Venkat Narayanaswamy (NCSU)

Postdoctoral Scholars

Qili Liu (UIUC)

Graduate Students

Damiano Baccarella (Ph.D. student, UIUC)

Brendan J. McGann (Ph.D. student, UIUC)

Michael D. Leonard (Ph.D. student, NCSU)

8. PUBLICATIONS

Following publications have been published and/or submitted with support from this grant in the second year of the project.

Refereed Journals

1. D. Baccarella, Q. Liu, B. McGann, G. Lee, T. Lee, Isolator-combustor interactions in a circular model scramjet with thermal and non-thermal choking-induced unstart, Journal of Fluid Mechanics, 917, A38-1, (2021)
2. D. Baccarella, Q. Liu, B. McGann, T. Lee, Combustion Induced Choking and Unstart Initiation in a Circular Constant-Area Supersonic Flow, AIAA Journal, 57, 12, 5365 (2019)
3. Q. Liu, D. Baccarella, B. McGann, T. Lee, Dual-Mode Operation and Transition in Axisymmetric Scramjets, AIAA Journal, 57, 11, 4764-4777 (2019)

4. Q. Liu, D. Bacarella, B. McGann, T. Lee, Cavity-enhanced combustion stability in an axisymmetric scramjet model, AIAA Journal, https://doi.org/10.2514/1.J058204 (2019).
5. Q. Liu, D. Baccarella, W. Landsberg, A. Veeraragaven, T. Lee, Cavity Flameholding in an Optical Axisymmetric Scramjet in Mach 4.5 Flows, Proc. Comb. Symp. 37, 3, 3733-3740 (2019)
6. D. Bacarella, Q. Liu, B. McGann, G. Lee, T. Lee, Isolator-combustor interactions in a circular model scramjet with thermal and non-thermal choking-induced unstart, Journal of Fluid Mechanics, Volume 917 (2021)

Conference Proceedings

1. D. Baccarella, G. Lee, Q. Liu, G. Elliott, J. Freund, T. Lee, Laser Induced Plasma Ignition Experiments in a Direct-Connect Supersonic Combustor at Mach 3, AIAA Propulsion and Energy Forum, Indianapolis IN, 19-22 August, 2019
2. Q. Liu, D. Baccarella, G. Lee, T. Lee, Influences of Cavity on Combustion Stabilization in an Axisymmetric Scramjet, AIAA SciTech, AIAA-2019-1681, 2019
3. N. Kato, G. Lee, T. Lee, A Comparison Between Axisymmetric and Perisymmetric Scramjet Flowpaths, AIAA SciTech 2022 (in-progress)

9. REFERENCES

1. Heiser W. H. and Pratt D. T., "Hypersonic air breathing propulsion," *AIAA Education Series*, Washington, D. C. USA, 1993.
2. C. Segal, The Scramjet Engine: Processes and Characteristics, Cambridge Aerospace Series, Cambridge University Press, 2009.
3. Im S., Baccarella D., McGann B., Liu Q., Wermer L. and Do H., "Unstart phenomena induced by mass addition and heat release in a model scramjet," *Journal of Fluid Mechanics*, Vol. 797, 2016, pp. 604-629.
4. M. R. Gruber, R. A. Baurle, T. Mathur, and K, Hsu, "Fundamental Studies of Cavity-Based Flameholder Concepts for Supersonic Combustors", Journal of Propulsionand Power, 17, 146-153 (2001).
5. C. C. Rasmussen, J. F. Driscoll, K. Hsu, J. Donbar, M. Gruber, and C. Carter, "Stability Limits of Cavity-Stabilized Flames in Supersonic Flow", Proceedings of the Combustion Institute, 30, 2825-2833 (2005).
6. T. Mathur, M. Gruber, K. Jackson, J. Donbar, W. Donaldson, T. Jackson, and F. Billig, "Supersonic Combusiton Experiments with a Cavity-Based Fuel Injector", Journal of Propulsionand Power, 17, 1305-1312 (2001).
7. Y. Tian, S. Yang, J. Le, F. Zhong, and X. Tian, "Investigation of Cmobustion Process of a Kerosene Fueled Combustor with Air Throttling", Combustion and Flmame 179, 74-85 (2017).
8. E. Jeong, I. Jeung, S. O'Byrne, and A. Houwing, "Investigation of Supersoinc Combustion with Angled Injection in a Cavity-Based Combustor", Journal of Propulsionand Power, **24**, 1258-1268 (2008).
9. F.S. Billig, "Design of Supersonic Combustors Based on Pressure-Area Fields," Symposium (International) on Combustion, 11, 755-769 (1967).
10. M.K. Smart, and C.A. Trexler, "Mach 4 Performance of Hypersonic Inlet with Rectangular-to-Elliptical Shape Transition", Journal of Propulsionand Power, 20, 288-293 (2004).

11. Z. Denman, W. Chan, S. Brieschenk, A. Veeraragavan, V. Wheatly, and M. Smart, "Ignition Experiments of Hydrocarbons in a Mach 8 Shape-Transitioning Scramjet Engine," Journal of Propulsionand Power, 32, 1462-1471 (2016).
12. Z. Denman, V. Wheatly, M. Smart, and A. Veeraragavan, "Supersonic Combusiton of Hydrocarbons in a Shape-Transitioning Hypersonic Engine," Proceedings of the Combustion Institute, 36, 2883-2891 (2017).
13. M. Gruber, S. Smith, and T. Mathur, "Experimental Characterization of Hydrocarbon-fueled Axisymmetric Scramjet Combustor Flowpaths," 17th AIAA International Space Planes and Hypersonic Systems and Technologies Conference, San Francisco, California (2011).
14. D. Riggins, R. Tackett, and T. Taylor, "Thermodynamic Analysis of Dual-Mode Scramjet Engine Operation and Performance," 14th AIAA/AHI Space Planes and Hypersonic Systems and Technologies Conference (2006).
15. W. Yao, Y. Yuan, X. Li, J. Wang, K. Wu, X. Fan, "Comparative Study of Elliptic and Round Scramjet Combustors Fueled by RP-3," Journal of Propulsion and Power, 34, 772-786 (2018).
16. Baccarella, D., Liu, Q., Lee, T., Hammack, S. D., and Do, H., "The supersonic combustion facility ACT-2," 55th AIAA Aerospace Sciences Meeting, AIAA SciTech Forum, AIAA, Grapevine, TX, 2017, p. 0103. doi:10.2514/3.50600.
17. Norris G., "X-51A scramjet fails on second attempt," *Aviation Week*, June 15th, 2011.
18. Ikui, T., Matsuo, K., and Nagai, M., "The mechanism of pseudo-shock waves," *Bulletin of the Japan Society of Mechanical Engineers*, Vol. 17, No. 108, 1974, pp. 731–739.
19. Matsuo, K., Miyazato, Y., and Kim, H. D., "Shock train and pseudo-shock phenomena in internal gas flows," *Progress in Aerospace Sciences*, Vol. 35, No. 1, 1999, pp. 33-100.
20. Gnani, F., Zare-Behtash, H., and Kontis, K., "Pseudo-shock waves and their interactions in high-speed intakes," *Progress in Aerospace Sciences*, Vol. 82, April 2016, pp. 36-56.
21. Tamaki, T., Tomita, Y., and Yamane, R., "A study of pseudo-shock, 1st report, λ-type pseudo-shock," *Bulletin of the Japan Society of Mechanical Engineers*, Vol. 13, No. 55, 1970, pp. 51–58.
22. Tamaki, T., Tomita, Y., and Yamane, R., "A study of pseudo-shock, 2nd report X-type pseudo-shock," *Bulletin of the Japan Society of Mechanical Engineers*, Vol. 14, No. 74, 1971, pp. 807–817.
23. Waltrup, P. J., and Billig, F. S., "Structure of shock waves in cylindrical ducts," *AIAA Journal*, Vol. 11, No. 10, 1973, pp. 1404–1408.
24. Smart M. K., "Flow modeling of pseudoshocks in backpressured ducts," *AIAA Journal*, Vol. 47, No. 4, 2009, pp. 1050-1053.
25. Wieting, A. R., "Exploratory study of transient unstart phenomena in a three-dimensional fixed-geometry scramjet engine," NASA Technical Note TN D-8156, 1976.
26. Rodi, P. E., Emami, S., and Trexler, C. A., "Unsteady pressure behaviour in a ramjet/scramjet inlet," *Journal of Propulsion and Power,* Vol. 12, No. 3, 1996, pp. 486-493.
27. Emami, S., Trexler, C. A., Auslender, A. H., and Weidner, J. P., "Experimental investigation of inlet-combustor isolators for a dual-mode scramjet at a Mach number of 4," NASA Technical Paper 3502, 1995.
28. Tan, H.-J., and Guo, R. W., "Experimental study of the unstable-unstarted condition of a hypersonic inlet at Mach 6," *Journal of Propulsion and Power,* Vol. 23, No. 4, 2007, pp. 783-788.

29. Wagner, J. L., Yuceil, K. B., Valdivia, A., Clemens, N., T., and Dolling D. S., "Experimental investigation of unstart in an inlet/isolator model in Mach 5 flow," *AIAA Journal*, Vol. 47, No. 6, 2009, pp. 1528-1542.
30. Zhang, Q. F., Tan, H. J., Sun, S., Bu, H. X., and Rao, C. Y., "Unstart of a hypersonic inlet with side compression caused by downstream choking," *AIAA Journal,* Vol. 54, No. 1, 2016, pp. 28-38.
31. Do, H., Im, S., Mungal, M. G., and Cappelli, M. A., "The influence of boundary layers on supersonic inlet flow unstart induced by mass injection," *Experiments in Fluids*, Vol. 51, No. 3, 2011, pp. 679-691.
32. Im S., Baccarella D., McGann B., Liu Q., Wermer L. and Do H., "Unstart phenomena induced by mass addition and heat release in a model scramjet," *Journal of Fluid Mechanics*, Vol. 797, 2016, pp. 604-629.
33. Ikui, T., Matsuo, K., Nagai, M., and Honjo, M., "Oscillation phenomena of pseudo-shock waves," *Bulletin of the JSME*, Vol. 17, No. 112, 1974, pp. 1278-1285.
34. Clemens, N. T., and Narayanaswamy, V., "Low-Frequency Unsteadiness of Shock Wave/Turbulent Boundary Layer Interactions," *Annual Reviews of Fluid Mechanics*, Vol. 46, 2014, pp. 469-492.
35. Klomparens, R. L., Driscoll J. F., and Gamba, M., "Unsteadiness characteristics and pressure distribution of an oblique shock train," AIAA Paper 2015-1519.
36. Xiong, B., Wang, Z., Fan., X., and Wang, Y., "Experimental study on the flow separation and self-excited oscillation phenomenon in a rectangular duct," *Acta Astronautica,* Vol. 133, 2017, pp. 158-165.
37. Frost M. A., Gangurde, D. Y., Paull, A., and Mee, D. J., "Boundary-layer separation due to combustion-induced pressure rise in supersonic flow," *AIAA Journal*, Vol. 47, No. 4, 2009, pp. 1050-1053.
38. Laurence, S. J., Karl, S., Martinez Schramm, J., and Hannemann, K., "Transient fluid-combustion phenomena in a model scramjet," *Journal of Fluid Mechanics,* Vol. 722, 2013, pp. 85-120.
39. Laurence, S. J., Lieber, D., Martinez Schramm, J., Hannemann, K., and Larsson, J., "Incipient thermal choking and stable shock-train formation in the heat-release region of a scramjet combustor. Part I: Shock tunnel experiments," *Combustion and Flame,* Vol. 162, No. 4, 2014, pp. 921-931.
40. O'Byrne, S., Doolan, M., Olsen, S. R., and Houwing, A. F. P., "Transient thermal choking processes in a model scramjet engine," *Journal of Propulsion and Power,* Vol. 16, No. 5, 2000, pp. 808-814.
41. Owens, M. G., Mullagiri, S., Segal, C., Ortwerth, P. J., and Mathur, A. B., "Thermal choking analyses in a supersonic combustor," *Journal of Propulsion and Power,* Vol. 17, No. 3, 2001, pp. 611-616.
42. Mashio S., Kurashina K., Bamba, T., Okimoto, S., and Kaji S., "Unstart phenomenon due to thermal choke in scramjet module," AIAA Paper 2001-1887.
43. Do H., Passaro A. and Baccarella D., "Inlet unstart of an ethylene-fueled model scramjet with a Mach 4.5 freestream flow," AIAA Paper 2012-5929.
44. Liu, Q., Baccarella, D., McGann, B. J., and Lee, T., "Experimental investigation of single jet and dual jet injection in a supersonic combustor," 2018 AIAA Aerospace Sciences Meeting, AIAA SciTech Forum, AIAA, Kissimmee, FL, 2018, p. 1363. doi:10.2514/6.2018-1363.

45. Liu, Q., Baccarella, D., Landsberg,W., Veeraragavan, A., and Lee, T., “Cavity flameholding in an optical axisymmetric scramjet in Mach 4.5 flows,” Proceedings of the Combustion Institute, 2018. doi:10.1016/j.proci.2018.08.037.
46. Lee, G., Liu, Q., Baccarella, D., Elliott, G. S., and Lee, T., “A novel supersonic injection scheme for laser induced breakdown ignition,” 2018 Aerodynamic Measurement Technology and Ground Testing Conference, AIAA Aviation Forum, AIAA, Atlanta, GA, 2018, p. 4286. doi:10.2514/6.2018-4286.
47. Sutton, K., and Graves, R. A., “A general stagnation-point convective-heating equation for arbitrary gas mixtures,” Tech. Rep. NASA TR R-376, NASA, 1971.
48. Baccarella, D., Liu, Q., McGann, B. J., and Lee, T., “Combustion Induced Choking and Unstart Initiation in a Circular Constant-Area Supersonic Flow,” AIAA Journal, Vol. under review, 2019.
49. Seitzman, J. M., and Hanson, R. K., “Comparison of excitation techniques for quantitative fluorescence imaging of reacting flows,” AIAA Journal, Vol. 31, No. 3, 1993, pp. 513–519. doi:10.2514/3.11359.
50. Kychakoff, G., Howe, R. D., and Hanson, R. K., “Quantitative flow visualization technique for measurements in combustion gases,” Applied Optics, Vol. 23, No. 5, 1984, pp. 704–712. doi:10.1364/AO.23.000704.
51. Baccarella, D., Liu, Q., McGann, B. J., and Lee, T., “Isolator Shock Dynamics of Mass Injection-Induced Unstart in a Circular Model Scramjet,” TBD, 2019.
52. A. Ben-Yakar, and R.K. Hanson, "Cavity Flame-Holders for Ignition and Flame Stabilization in Scramjets: An Overview", Journal of Propulsionand Power, 17, 869-877 (2001).
53. A. H. Shapiro, The Dynamics and Thermodynamics of Compressible Flow Volume I, Wiley, New York: The Ronald Press Company, 1953.
54. Crocco, L., *One Dimensional Treatment of Steady Gas Dynamics*, edited by Emmons, H. W., Fundamentals of Gas Dynamics, Princeton Univ. Press, Princeton, NJ, 1958, pp. 110–130.